Anisotropy ansatz for the axisymmetric Jeans equations

Leonardo De Deo [1,2,3]★ Luca Ciotti [1] and Silvia Pellegrini [1,2]

[1]*Department of Physics and Astronomy, University of Bologna, Via Gobetti 93/2, I-40129 Bologna, Italy*
[2]*Istituto Nazionale di Astrofisica (INAF), Osservatorio di Astrofisica e Scienza dello Spazio di Bologna (OAS), Via Gobetti 93/3, I-40129 Bologna, Italy*
[3]*International PhD College – Collegio Superiore, University of Bologna, I-40129 Bologna, Italy*

ABSTRACT

The Jeans equations do not form a closed system, and to solve them a parametrization relating the velocity moments is often adopted. For axisymmetric models, a phenomenological choice (the 'b-ansatz') is widely used for the relation between the vertical (σ_z^2) and radial (σ_R^2) components of the velocity dispersion tensor, thus breaking their identity present in two-integral systems. However, the way in which the ansatz affects the resulting kinematical fields can be quite complicated, so that the analysis of these fields is usually performed only after numerically computing them. We present here a general procedure to study the properties of the ansatz-dependent fields $\overline{v_\varphi^2}$, $\Delta = \overline{v_\varphi^2} - \sigma_z^2$ and $\Delta_R = \overline{v_\varphi^2} - \sigma_R^2$. Specifically, the effects of the b-ansatz can be determined before solving the Jeans equations once the behaviour over the (R, z)-plane of three easy-to-build ansatz-independent functions is known. The procedure also constrains the ansatz to exclude unphysical results (as a negative $\overline{v_\varphi^2}$). The method is illustrated by discussing the cases of three well-known galaxy models: the Miyamoto & Nagai and Satoh discs, and the Binney logarithmic halo, for which the regions and the constraints on the ansatz values can be determined analytically; a two-component (Miyamoto & Nagai plus logarithmic halo) model is also discussed.

Key words: galaxies: elliptical and lenticular, cD – galaxies: kinematics and dynamics – galaxies: structure.

1 INTRODUCTION

The Jeans equations (hereafter JEs) are one of the standard tools for the modelling of stellar systems (e.g. Binney & Tremaine 2008, hereafter BT08; see also Ciotti 2021, hereafter C21) and to extract information from observations (e.g. Scott et al. 2015; Cappellari 2016; Li et al. 2016; Zhu et al. 2023). However, the JEs are moments of the more fundamental Boltzmann equation, and in the collisionless limit they suffer in general from a 'closure problem'. Their closure can be obtained by assuming a (more or less motivated) dependence of the phase-space distribution function (hereafter DF) on the available integrals of motion. Alternatively, some relation between the velocity moments (usually between the velocity dispersion tensor components) can be imposed through some phenomenological 'ansatz'. This latter approach is not as elegant and physically sound as deriving all the model properties from the DF, coupled with the Poisson equation and asking for self-consistency (e.g. King 1963; Stiavelli & Bertin 1985; Bertin & Varri 2008), or using a DF built from actions (e.g. Binney 2010; see also Posti et al. 2015; Binney & Vasiliev 2023), or reconstructing the DF numerically with the Schwarzschild orbital superposition method (Schwarzschild 1979; see also, e.g. Statler 1987; Cappellari et al. 2007; Thomas et al. 2009). However, the methods mentioned above are not always well suited for exploratory works because in general the solution of the self-consistency problem requires non-trivial numerical work.

An important advantage of using the JEs is that the stellar density distribution of the model can be chosen at the beginning to be in good agreement with the observational data (e.g. by using specific density profiles or by multicomponent modelling), and that the closure ansatz guarantees some direct control on the resulting kinematics. Of course, the problem of the existence of a non-negative DF for the obtained model remains in general open.

In this work, we address two aspects worth a thorough investigation, both related to how a widely used closure ansatz (the b-ansatz; Cappellari 2008) affects the solutions of the JEs: the first is to formalize a general procedure, to be applied before solving the equations, to determine the constraints on this ansatz, as for example those coming from the request of positivity of $\overline{v_\varphi^2}$, thus avoiding repeated and time-consuming numerical tests. The second is to gain some qualitative understanding of its effects on the kinematical fields, before their construction. Moreover, as a widely used decomposition of $\overline{v_\varphi^2}$ (e.g. that proposed by Satoh 1980, and its variants) requires the positivity of certain functions, we also determine the conditions for its applicability.

The paper is organized as follows: in Sections 2 and 3, after reviewing the JEs for two-integral axisymmetric systems, the general solutions with the b-ansatz, relating the vertical (σ_z^2) and the radial (σ_R^2) velocity dispersions, are derived, and cast in a form suitable for the successive investigation. In Section 4, we determine the constraints on the ansatz to assure the positivity of $\overline{v_\varphi^2}$ and to use the Satoh decomposition and its generalizations. In Sections 5 and 6, we apply the procedure to some well-known galaxy models, for which a fully analytical treatment is possible: the Miyamoto &

Nagai and Satoh discs, and the Binney logarithmic halo. A more realistic two-component model, made by a stellar Miyamoto & Nagai disc embedded in a dark matter Binney halo, is also discussed. In Section 7, the main results are summarized.

2 TWO-INTEGRAL SYSTEMS

As is well known, the JEs for an axisymmetric stellar system described by a two-integral DF $f = f(E, J_z)$, where E and J_z are respectively the orbital energy and the axial angular momentum, are

$$\begin{cases} \dfrac{\partial \rho_* \sigma_z^2}{\partial z} = -\rho_* \dfrac{\partial \Phi}{\partial z}, \\[2mm] \dfrac{\partial \rho_* \sigma_z^2}{\partial R} - \dfrac{\rho_* \Delta}{R} = -\rho_* \dfrac{\partial \Phi}{\partial R}, \quad \Delta \equiv \overline{v_\varphi^2} - \sigma_z^2, \end{cases} \tag{1}$$

(see e.g. BT08; C21): $\rho_*(R, z)$ and $\Phi(R, z)$ are the stellar density distribution and the total (e.g. stars, plus dark matter) gravitational potential. Standard cylindrical coordinates are used, σ_z^2 is the vertical velocity dispersion, and a bar over a symbol indicates the average over velocity in phase space. In particular, $\overline{v_\varphi^2} = \overline{v_\varphi}^2 + \sigma_\varphi^2$, where $\overline{v_\varphi}$ is the streaming velocity field in the azimuthal direction, and σ_φ^2 is the azimuthal velocity dispersion. Finally, the only non-vanishing ordered velocity field is $\overline{v_\varphi}$, while $\overline{v_R} = \overline{v_z} = 0$; moreover, $\sigma_R^2 = \sigma_z^2$, and all the mixed components of the velocity dispersion tensor vanish.

The solutions of equation (1) with null boundary conditions at infinity are

$$\begin{cases} \rho_* \sigma_z^2 = \displaystyle\int_z^\infty \rho_* \dfrac{\partial \Phi}{\partial z'} dz', \\[3mm] \dfrac{\rho_* \Delta}{R} = \dfrac{\partial \rho_* \sigma_z^2}{\partial R} + \rho_* \dfrac{\partial \Phi}{\partial R} = [\rho_*, \Phi], \end{cases} \tag{2}$$

where

$$[\rho_*, \Phi] \equiv \int_z^\infty \left(\frac{\partial \rho_*}{\partial R} \frac{\partial \Phi}{\partial z'} - \frac{\partial \rho_*}{\partial z'} \frac{\partial \Phi}{\partial R} \right) dz', \tag{3}$$

is a commutator-like operator (see e.g. Barnabè et al. 2006; see also C21 and references therein). From the second of equation (), Δ can be obtained by differentiation of $\rho_* \sigma_z^2$ or by integration of the commutator, as in equation (3). This latter approach is to be preferred, as it usually reveals important properties of the solutions that are not apparent in the first approach based on differentiation: for example, it is immediate to show that the commutator vanishes for a spherical density $\rho_*(r)$ in a spherical total potential $\Phi(r)$ and that, in the case of ellipsoidal densities in ellipsoidal potentials, the commutator is everywhere positive (negative) when the density shape is flatter (rounder) than the potential (see e.g. C21). Of course, when using the commutator for the computation of Δ, the radial derivative of $\rho_* \sigma_z^2$ is obtained as a byproduct:

$$D \equiv \frac{\partial \rho_* \sigma_z^2}{\partial R} = [\rho_*, \Phi] - \rho_* \frac{\partial \Phi}{\partial R}, \tag{4}$$

an identity we will use in the following. Once σ_z^2 and Δ are known, one has

$$\overline{v_\varphi^2} = \Delta + \sigma_z^2 = \frac{[R\rho_*, \Phi]}{\rho_*}, \tag{5}$$

where the second identity involving again a commutator can be easily proved from equations (2) and (3).

Notice that a model with $\overline{v_\varphi^2} < 0$ somewhere is certainly physically inconsistent, but $\overline{v_\varphi^2} \geq 0$ everywhere is not a sufficient condition for

consistency: as is well known, there are models with 'acceptable' solutions of the JEs and a negative (unphysical) DF (see e.g. Ciotti & Pellegrini 1992; see also Chapter 14 in C21, and references therein).

2.1 The Satoh k-decomposition

For axisymmetric models with $\Delta \geq 0$ everywhere, Satoh (1980) introduced the widely used k-decomposition of $\overline{v_\varphi^2}$:

$$\overline{v_\varphi} = k\sqrt{\Delta}, \quad \sigma_\varphi^2 = \sigma_z^2 + (1 - k^2)\Delta, \tag{6}$$

where k is constant with $0 \leq k^2 \leq 1$. If $k = 0$, then $\overline{v_\varphi} = 0$ and no net rotation is present, while, if $k^2 = 1$, then $\sigma_\varphi^2 = \sigma_z^2$ and the system is an isotropic rotator. Moreover, if $\Delta = 0$ (as for spherical models), then no ordered rotation is possible, and the system is isotropic independently of k.

As shown in Ciotti & Pellegrini (1996), the original Satoh decomposition can be easily generalized to assume a spatially dependent $k(R, z)$, provided that

$$k^2(R, z) \leq k_M^2(R, z) \equiv \frac{\overline{v_\varphi^2}}{\Delta}, \tag{7}$$

where the upper limit k_M^2 corresponds to maximally rotating models with no net velocity dispersion in the azimuthal direction, and is then obtained from equation (6) imposing $\sigma_\varphi^2 = 0$ everywhere; in this case, the density flattening is fully supported by the streaming velocity field $\overline{v_\varphi}$. Of course, k is not required to be positive, thus allowing the modelling of counter-rotating structures with negative $\overline{v_\varphi}$ (see e.g. Negri, Pellegrini & Ciotti 2013).

In Appendix A1, we discuss the most general decomposition for $\overline{v_\varphi^2}$, which holds also for models with $\Delta < 0$.

3 MORE GENERAL SYSTEMS

Having assessed the classical case of two-integral axisymmetric systems, we now turn to the focus of the paper, i.e. the study of the properties of the kinematical fields associated with more general ansatz distinguishing between σ_z^2 and σ_R^2, and so implicitly based on a DF with a third integral in addition to E and J_z. If the third integral is an even function of v_z and v_R, the first of equation (1) remains unchanged, while the second becomes (Cappellari 2008; C21):

$$\frac{\partial \rho_* \sigma_R^2}{\partial R} - \frac{\rho_* \Delta_R}{R} = -\rho_* \frac{\partial \Phi}{\partial R}, \quad \Delta_R \equiv \overline{v_\varphi^2} - \sigma_R^2. \tag{8}$$

Notice that, in addition to σ_z^2, all quantities depending on ρ_* and Φ, such as the commutator $[\rho_*, \Phi]$ and the function D in equation (4), remain the same as in the two-integral case.

Different ansatz can be introduced to solve equation (8), which is independent of the vertical velocity dispersion, and contains the two unknown functions $\overline{v_\varphi^2}$ and σ_R^2. In the following, we study in detail the 'b-ansatz', relating σ_R^2 with σ_z^2. Introduced by Cappellari (2008), it was adopted for the Jeans Anisotropic Modelling method (JAM; see also Cappellari 2020), which is widely used to reproduce the properties of observed galaxies (e.g. Cappellari et al. 2013; Zhu et al. 2016; Loubser et al. 2020; Nitschai et al. 2021; Surti et al. 2024). This solution of the JEs, implying the alignment of the velocity ellipsoid with the cylindrical coordinates, was presented as an efficient modelling able to capture the main properties of the velocity ellipsoid inferred from extensive three-integral Schwarzschild's modelling of integral-field stellar kinematics, under the mass-follows-light hypothesis (Cappellari 2008). The main motivation for the adoption of the 'b-ansatz', in fact, is that it allows to model adequately

the observations, in particular the integral-field spectroscopy of axisymmetric galaxies classified as regular rotators and stellar discs (see sections 2.3 and 2.4 of Cappellari 2008; Cappellari 2016). Of course, on the theoretical side, the *b*-ansatz is not the only one possible, and in Appendix A2 we present the 'μ-ansatz', leading to a nice closure of equation (8).

3.1 The *b*-ansatz

In the '*b*-ansatz', the unknown σ_R^2 is linked to σ_z^2 through the choice of the function $b(R, z) \geq 0$, as

$$\sigma_R^2 = b(R, z)\sigma_z^2. \tag{9}$$

When $b = 0$, the system has no radial velocity dispersion, while $b = 1$ gives the two-integral case.

Inserting equation (9) into equation (8), recalling the definition of D in equation (4), and solving for Δ_R, we obtain

$$\frac{\rho_* \Delta_R}{R} - \rho_* \sigma_z^2 \frac{\partial b}{\partial R} = bD + \rho_* \frac{\partial \Phi}{\partial R} =$$
$$b [\rho_*, \Phi] + (1 - b)\rho_* \frac{\partial \Phi}{\partial R}, \tag{10}$$

where in the last expression we have used again equation (4). Note how b multiplies functions that are *independent* of the adopted ansatz.

Once Δ_R is known, if we restrict to a b function that depends only on z (or to a constant b, a special case commonly used), $\partial b/\partial R = 0$ on the l.h.s. of equation (10), and

$$\overline{v_\varphi^2} = \Delta_R + b\sigma_z^2 = bB + R\frac{\partial \Phi}{\partial R} =$$
$$b \frac{[R\rho_*, \Phi]}{\rho_*} + (1 - b)R\frac{\partial \Phi}{\partial R}, \tag{11}$$

where from equation (4)

$$B \equiv \frac{R D}{\rho_*} + \sigma_z^2 = \frac{[R\rho_*, \Phi]}{\rho_*} - R\frac{\partial \Phi}{\partial R}. \tag{12}$$

Only $b(z)$ functions leading to $\overline{v_\varphi^2} \geq 0$ everywhere are physically acceptable, and Section 4.1 deals with this request.

Finally, from equation (11), we obtain:

$$\Delta = \overline{v_\varphi^2} - \sigma_z^2 = \Delta_R + (b - 1)\sigma_z^2 = bB + C, \tag{13}$$

where from equations (4) and (12)

$$C \equiv R\frac{\partial \Phi}{\partial R} - \sigma_z^2 = \frac{R [\rho_*, \Phi]}{\rho_*} - B. \tag{14}$$

From equation (13), if $\Delta_R \geq 0$ and $b(z) \geq 1$, then $\Delta \geq 0$, and if $\Delta_R < 0$ and $b(z) \leq 1$, then $\Delta < 0$. A complete discussion on the conditions for the positivity of Δ_R and Δ is given in Sections 4.2 and 4.3. Notice that the values of Δ in the *b*-ansatz are not the same of the two-integral case, because, with the introduction of the ansatz, σ_z^2 remains unaltered, but $\overline{v_\varphi^2}$ changes. Also important, the functions D, B, and C are ansatz-independent.

Models with $\Delta_R \geq 0$ allow for a *k*-decomposition of $\overline{v_\varphi^2}$ similar to that in equation (6), i.e. (Cappellari 2008):

$$\overline{v_\varphi} = k\sqrt{\Delta_R}, \quad \sigma_\varphi^2 = \sigma_R^2 + (1 - k^2)\Delta_R. \tag{15}$$

Whenever $k^2 < 1$, one has $\sigma_\varphi^2 > \sigma_R^2$, i.e. the orbital anisotropy is tangential; radial anisotropy ($\sigma_\varphi^2 < \sigma_R^2$) requires $k^2 > 1$. Of course, the decomposition in equation (6) can also be applied, where now Δ is given in equation (13), provided that $\Delta \geq 0$ everywhere.

A different decomposition for the azimuthal motions can be given by choosing the parameter γ, introduced in Cappellari et al. (2007):

$$\gamma = 1 - \frac{\sigma_\varphi^2}{\sigma_R^2}, \quad \overline{v_\varphi^2} = \Delta_R + \gamma\sigma_R^2, \tag{16}$$

where clearly

$$-\frac{\Delta_R}{\sigma_R^2} \leq \gamma \leq 1, \tag{17}$$

with the first inequality required for $\overline{v_\varphi^2} \geq 0$. Positive γ values correspond to radial anisotropy, while $\gamma < 0$ gives tangential anisotropy; in two-integral systems, $\gamma = 0$ corresponds to the isotropic case. Notice that, from equation (17), γ can be either positive or negative if $\Delta_R > 0$; instead, if $\Delta_R < 0$, γ cannot be taken negative, i.e. the velocity dispersion tensor can only be radially anisotropic. In Section 7, some findings based on the use of this decomposition to interpret recent observations (Wang, Cappellari & Peng 2021) are discussed in light of our analysis.

4 PHYSICAL CONSTRAINTS ON THE ANSATZ

Equation (8) can be solved only with the introduction of some closure, as those presented in Section 3.1 or Appendix A2. However, arbitrary ansatz functions can lead to unphysical solutions of the JEs, such as negative values of $\overline{v_\varphi^2}$. Therefore, it would be useful to know in advance (i.e. before solving the equations) what constraints must be imposed on the ansatz function in order to avoid unphysical solutions, and also how specific choices of the ansatz functions affect the properties of the solutions in different regions of space. This section is dedicated to these problems.

In practice, being $\sigma_z^2 \geq 0$ independent of the ansatz, the positivity of σ_R^2 is guaranteed by equation (9); therefore, we focus on the positivity of $\overline{v_\varphi^2}$ only. Information on the sign of Δ and Δ_R is also relevant for the modelling because, although not directly related to model consistency, their positivity is needed to apply a decomposition of $\overline{v_\varphi^2}$ as those in equations (6) and (15).

In the following, we restrict for simplicity to models with $\partial \Phi/\partial R \geq 0$ everywhere (the most common situation), and we limit to consider $b = b(z)$; finally, we indicate with P = (R, z) a generic point in the (R, z)-plane.

4.1 Positivity of $\overline{v_\varphi^2}$: the $\mathscr{B}$ region

We discuss here the positivity of $\overline{v_\varphi^2}$, a condition necessary to model consistency. Introducing the sets

$$\mathscr{B}^\pm = \{(R, z) : B \gtrless 0\}, \quad \mathscr{B}^0 = \{(R, z) : B = 0\}, \tag{18}$$

equation (11) shows that, independently of $b(z)$, $\overline{v_\varphi^2} \geq 0$ over the region $\mathscr{B}^{+0} = \mathscr{B}^+ \cup \mathscr{B}^0$. Instead, the behaviour of B over $\mathscr{B}^-$ constrains the possible choices of $b(z)$, as we now describe. We indicate with $\text{Pr}(\mathscr{B}^\pm)$ the *projection* of $\mathscr{B}^\pm$ on the z-axis, and with $\mathscr{B}_z^\pm = \{R : B \gtrless 0, z \in \text{Pr}(\mathscr{B}^\pm)\}$ the *radial section* at fixed z of $\mathscr{B}^\pm$ (see Fig. 1 for a qualitative illustration). As we restrict to systems with a reflection symmetry about the equatorial plane, without loss of generality, in the following we limit the discussion to $z \geq 0$. From equation (11), the condition $\overline{v_\varphi^2} \geq 0$ over $\mathscr{B}^-$ is guaranteed provided that, at each $z \in \text{Pr}(\mathscr{B}^-)$,

$$b(z) \leq b_M(z) \equiv \min_{\mathscr{B}_z^-} \frac{R}{|B|} \frac{\partial \Phi}{\partial R}$$
$$= \min_{\mathscr{B}_z^-} \left(1 + \frac{R [\rho_*, \Phi] + \rho_* \sigma_z^2}{\rho_* |B|}\right), \quad z \in \text{Pr}(\mathscr{B}^-), \tag{19}$$
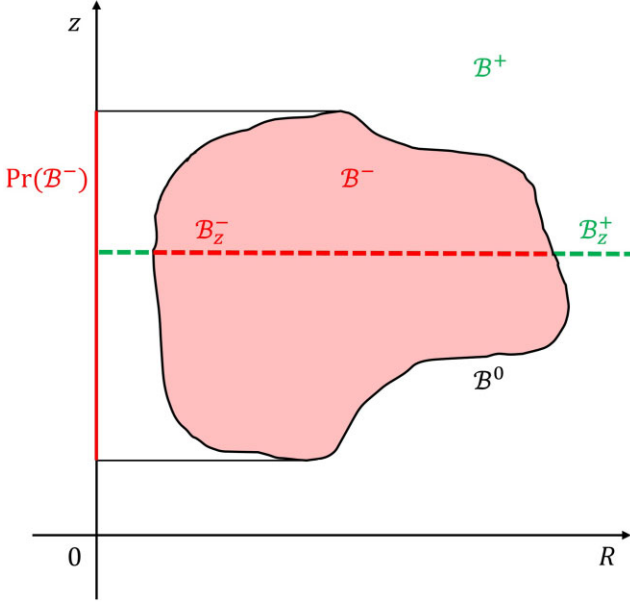
Figure 1. Cartoon of a fictitious $\mathscr{B}^-$ region (red), together with its projection on the z-axis $\mathrm{Pr}(\mathscr{B}^-)$, a radial section $\mathscr{B}_z^-$ (red dashed line), and its complement $\mathscr{B}_z^+$ (green dashed line). From equation (18), $\mathscr{B}^+ \cup \mathscr{B}^- \cup \mathscr{B}^0$ fully covers the (R, z)-plane.

where the last equality has been obtained using equation (14). Notice that the independence of b from R implies that the upper limit $b_{\mathrm{M}}(z)$, determined over $\mathscr{B}_z^-$, applies also to points in the complementary section $\mathscr{B}_z^+$: therefore, the function $b_{\mathrm{M}}(z)$ provides a constraint over the whole *rectangular strip* defined by $R \geq 0$ and $z \in \mathrm{Pr}(\mathscr{B}^-)$. From now on, we will refer to this region as 'the strip $\mathrm{Pr}(\mathscr{B}^-)$'. In the special case of a constant b, the condition in equation (19) reduces to $b \leq b_{\mathrm{M}}$, where b_{M} is the minimum of $b_{\mathrm{M}}(z)$.

4.2 Positivity of Δ_R: the $\mathscr{D}$ region

As seen in Section 3.1, the necessary condition to apply the k-decomposition to $\overline{v_\varphi^2}$ is to have $\Delta_R \geq 0$ or $\Delta \geq 0$. Introducing the sets

$$\mathscr{D}^\pm = \{(R, z) : D \gtrless 0\}, \quad \mathscr{D}^0 = \{(R, z) : D = 0\}, \tag{20}$$

where D is defined in equation (4), the first of equation (10) (where now $\partial b / \partial R = 0$) shows that, independently of $b(z)$, $\Delta_R \geq 0$ over the region $\mathscr{D}^{+0} = \mathscr{D}^+ \cup \mathscr{D}^0$. Instead, the condition $\Delta_R \geq 0$ over $\mathscr{D}^-$ requires

$$b(z) \leq b_0(z) \quad \equiv \min_{\mathscr{D}_z^-} \frac{\rho_*}{|D|} \frac{\partial \Phi}{\partial R} =$$
$$= \min_{\mathscr{D}_z^-} \left(1 + \frac{[\rho_*, \Phi]}{|D|} \right), \quad z \in \mathrm{Pr}(\mathscr{D}^-), \tag{21}$$

where $\mathrm{Pr}(\mathscr{D}^\pm)$ is the projection of $\mathscr{D}^\pm$ on the z-axis, $\mathscr{D}_z^\pm = \{R : D \gtrless 0, z \in \mathrm{Pr}(\mathscr{D}^\pm)\}$, and the last equality follows from equation (4). Due to the independence of b from R, the condition in equation (21) must be verified over the whole strip $\mathrm{Pr}(\mathscr{D}^-)$. In the special case of a constant b, then $\Delta_R \geq 0$ for $b \leq b_0$, where b_0 is the minimum of $b_0(z)$.

Notice that from Theorem B.1 the strip $\mathrm{Pr}(\mathscr{B}^-)$ is contained in the strip $\mathrm{Pr}(\mathscr{D}^-)$, and in this common region $b_0(z) \leq b_{\mathrm{M}}(z)$, as proved in Theorem B.4.

4.3 Positivity of Δ: the $\mathscr{C}$ region

The determination of the positivity of Δ as a function of $b(z)$ is more complicated, depending on the sign of both the B and C functions in equation (13). As done above, we introduce the sets

$$\mathscr{C}^\pm = \{(R, z) : C \gtrless 0\}, \quad \mathscr{C}^0 = \{(R, z) : C = 0\}, \tag{22}$$

and $\mathscr{C}_z^\pm = \{R : C \gtrless 0, z \in \mathrm{Pr}(\mathscr{C}^\pm)\}$; also, $\mathscr{C}^{+0} = \mathscr{C}^+ \cup \mathscr{C}^0$. The sign of Δ at a point P depends on its position in the (R, z)-plane, as follows:

(i) $\Delta \geq 0$ independently of $b(z)$ over $\mathscr{B}^{+0} \cap \mathscr{C}^{+0}$. Moreover, $\Delta \geq 0$ over $\mathscr{B}^+ \cap \mathscr{C}^-$ for

$$b(z) \geq b_1(z) \equiv \max_{\mathscr{B}_z^+ \cap \mathscr{C}_z^-} \frac{|C|}{B}$$
$$= \max_{\mathscr{B}_z^+ \cap \mathscr{C}_z^-} \left(1 - \frac{R[\rho_*, \Phi]}{\rho_* B} \right), \quad z \in \mathrm{Pr}(\mathscr{B}^+ \cap \mathscr{C}^-), \tag{23}$$

and over $\mathscr{B}^- \cap \mathscr{C}^+$ for

$$b(z) \leq b_2(z) \equiv \min_{\mathscr{B}_z^- \cap \mathscr{C}_z^+} \frac{C}{|B|}$$
$$= \min_{\mathscr{B}_z^- \cap \mathscr{C}_z^+} \left(1 + \frac{R[\rho_*, \Phi]}{\rho_*|B|} \right), \quad z \in \mathrm{Pr}(\mathscr{B}^- \cap \mathscr{C}^+). \tag{24}$$

(ii) $\Delta < 0$ independently of $b(z)$ over $(\mathscr{B}^- \cap \mathscr{C}^-) \cup (\mathscr{B}^0 \cap \mathscr{C}^-) \cup (\mathscr{B}^- \cap \mathscr{C}^0)$.[1] Moreover, $\Delta < 0$ over $\mathscr{B}^+ \cap \mathscr{C}^-$ for $b(z) < b_1(z)$, and over $\mathscr{B}^- \cap \mathscr{C}^+$ for $b(z) > b_2(z)$.

For a spatially constant b, the previous inequalities hold replacing $b_1(z)$ and $b_2(z)$ with b_1 and b_2, which are respectively the maximum of $b_1(z)$, and the minimum of $b_2(z)$.

Summarizing, independently of $b(z)$, $\overline{v_\varphi^2} \geq 0$ over $\mathscr{B}^{+0}$, $\Delta_R \geq 0$ over $\mathscr{D}^{+0}$, and $\Delta \geq 0$ over $\mathscr{B}^{+0} \cap \mathscr{C}^{+0}$, and $\Delta < 0$ over $(\mathscr{B}^- \cap \mathscr{C}^-) \cup (\mathscr{B}^0 \cap \mathscr{C}^-) \cup (\mathscr{B}^- \cap \mathscr{C}^0)$. Instead, equations (19), (21), (23), and (24) set the constraints on $b(z)$ required for the positivity of $\overline{v_\varphi^2}$ over $\mathscr{B}^-$, Δ_R over $\mathscr{D}^-$, and Δ over the intersection regions $\mathscr{B}^+ \cap \mathscr{C}^-$ and $\mathscr{B}^- \cap \mathscr{C}^+$.

4.4 Some general considerations

The properties of the kinematical fields resulting from a given choice for $b(z)$ are determined by the relations between the ansatz-independent regions $\mathscr{B}^\pm$, $\mathscr{C}^\pm$ and $\mathscr{D}^\pm$ and the functions defined over them. Each region is made by two disjoint parts fully covering the (R, z)-plane, thus the determination of just $\mathscr{B}^-$, $\mathscr{C}^-$ and $\mathscr{D}^-$ suffices for investigating a given model. In Appendix B, some general results about the relative positions of the regions and the constraints on $b(z)$ are presented. In particular, it is shown that $\mathscr{B}^-$ is always contained in $\mathscr{D}^-$. Moreover, if $[\rho_*, \Phi] > 0$ over the whole (R, z)-plane (as for oblate self-gravitating models), then $\mathscr{B}^- \subseteq \mathscr{C}^+$ and $\mathscr{C}^- \subseteq \mathscr{B}^+$; if $[\rho_*, \Phi] = 0$ everywhere (as in spherically symmetric models), then $\mathscr{B}^- = \mathscr{C}^+$, $\mathscr{B}^+ = \mathscr{C}^-$, and $\mathscr{D}^0$ coincides with the whole (R, z)-plane; if $[\rho_*, \Phi] < 0$ (as for prolate self-gravitating models), then $\mathscr{B}^+ \subseteq \mathscr{C}^-$, $\mathscr{C}^+ \subseteq \mathscr{B}^-$, and $\mathscr{D}^-$ coincides with the whole (R, z)-plane. Finally, from Theorems B.5 and B.7, it follows that for models with $[\rho_*, \Phi] \geq 0$ everywhere (a quite common situation), one

---

[1]This region is the complementary of the region in (i), minus the regions in equations (23) and (24), as can be proved with the De Morgan's law.

Figure 2. Scheme representing the behaviour, as a function of b, of the kinematical fields $\overline{v_\varphi^2}$, Δ_R, and Δ over the regions $\mathscr{B}^\pm$, $\mathscr{C}^\pm$, and $\mathscr{D}^\pm$, for a model with $[\rho, \Phi] > 0$. Each row refers to the indicated region; arrows point upwards if the field is increasing, and downwards if the field is decreasing for increasing b; black arrows indicate a positive value, and red arrows a negative one. For $b > b_M$, the model is unphysical.

has

$$
\begin{cases}
b_1(z) \leq 1, & \forall z \in \mathrm{Pr}(\mathscr{C}^-), \\
1 \leq b_0(z) \leq b_2(z) \leq b_M(z), & \forall z \in \mathrm{Pr}(\mathscr{B}^-).
\end{cases}
\tag{25}
$$

In this case, from the considerations above, $\mathscr{B}^-$ and $\mathscr{C}^-$ are disjoint, but this does not mean that the two projections in equation (25) are disjoint too: actually, they may coincide with the z-axis. In the special case of $[\rho_*, \Phi] = 0$ everywhere, in equation (25) we would have $b_1 = b_0 = b_2 = 1$.

We conclude with an example of the qualitative effects of an increase of b (for simplicity assumed as spatially constant) on σ_R^2, $\overline{v_\varphi^2}$, Δ_R, and Δ, in the various regions. Suppose a given model is assigned, and the regions $\mathscr{B}^\pm$, $\mathscr{C}^\pm$, and $\mathscr{D}^\pm$ have been determined; furthermore, suppose $[\rho_*, \Phi] \geq 0$ everywhere, so that equation (25) holds. We start considering the case of $b = 0$ (i.e. $\sigma_R^2 = 0$ everywhere): as 0 is smaller than b_0 and b_M, then $\overline{v_\varphi^2}$ and Δ_R are positive everywhere, while $\Delta < 0$ somewhere in $\mathscr{C}^-$ (because $0 < b_1$), and $\Delta \geq 0$ everywhere in $\mathscr{C}^+$ (because $0 < b_2$). For increasing b, σ_R^2 increases everywhere, $\overline{v_\varphi^2}$ decreases over $\mathscr{B}^-$ and increases over $\mathscr{B}^+$, while Δ_R decreases over $\mathscr{D}^-$ and increases over $\mathscr{D}^+$. As $\mathscr{B}^- \subseteq \mathscr{D}^-$, over $\mathscr{B}^-$ one has that Δ_R decreases because $\overline{v_\varphi^2}$ decreases and σ_R^2 increases; over the remaining part of $\mathscr{D}^-$ (i.e. $\mathscr{B}^+ \cap \mathscr{D}^-$), instead, Δ_R decreases, and so σ_R^2 increases more than $\overline{v_\varphi^2}$. Increasing further b above b_1, Δ becomes positive over $\mathscr{C}^-$, then when $b > b_0$, Δ_R becomes negative somewhere over $\mathscr{D}^-$, and for $b > b_2$, Δ becomes negative somewhere over $\mathscr{B}^-$; finally, for $b > b_M$, $\overline{v_\varphi^2} < 0$ somewhere in $\mathscr{B}^-$, and the model becomes unphysical. These behaviours are summarized in the table in Fig. 2.

5 ONE-COMPONENT MODELS

In light of the results in Section 4, we now explore the behaviour of some well-known galaxy models that allow for an almost complete analytical treatment, i.e. the Miyamoto & Nagai (1975) (hereafter MN) disc, the Satoh (1980) disc, and the Binney logarithmic halo (BT08). In Section 6, we then consider the case of the two-component model made by a stellar MN disc embedded in a dark matter Binney logarithmic halo.

5.1 The Miyamoto & Nagai disc

The potential–density pair of the MN disc of total mass M_*, and scale lengths a_* and b_*, can be written as

$$
\begin{cases}
\Phi_* = -\dfrac{GM_*}{b_*\xi}, & \xi \equiv \sqrt{R^2 + (s + \zeta)^2}, \\[2ex]
\rho_* = \dfrac{M_*}{b_*^3}\dfrac{s\xi^2 + 3\zeta(s+\zeta)^2}{4\pi\zeta^3\xi^5},
\end{cases}
\tag{26}
$$

where $\zeta \equiv \sqrt{1 + z^2}$, and $s \equiv a_*/b_*$ measures the flattening of the disc. For $a_* = 0$, the MN model reduces to the Plummer (1911) sphere, and for $b_* = 0$ to the razor-thin Kuzmin disc (Kuzmin 1956, Toomre 1963). In the formulae above and in this section, R and z are assumed to be normalized to $b_* \neq 0$.

From equations (2) and (3), we have:

$$
\rho_*\sigma_z^2 = \frac{GM_*^2}{b_*^4}\frac{(s+\zeta)^2}{8\pi\zeta^2\xi^6}, \quad [\rho_*, \Phi_*] = \frac{GM_*^2}{b_*^5}\frac{sR}{4\pi\zeta^3\xi^6}.
\tag{27}
$$

In particular, $[\rho_*, \Phi_*] \geq 0$ everywhere, vanishing in the spherical case ($s = 0$): therefore, equation (25) and the considerations made at the end of Section 4 apply. For reference, in the top panels of Fig. 3, we show the 2D maps of the ansatz-independent fields σ_z^2, $R[\rho_*, \Phi_*]/\rho_*$ (i.e. the Δ field in the two-integral case), and $R\partial\Phi/\partial R$, for a disc flattening of $s = 1$.

The first task to explore the model behaviour is the identification of the $\mathscr{B}$, $\mathscr{C}$, and $\mathscr{D}$ regions. Quite remarkably, equation (27) allows for an analytical expression of the B, C, and D functions:

$$
\mathscr{B}^- = \left\{ (R, z) : \sqrt{5}R - (s + \zeta) > 0 \right\},
\tag{28}
$$

i.e. $\mathscr{B}^-$ is the portion of the (R, z)-plane at the right of the hyperbola $\mathscr{B}^0$ with vertex $R = (1 + s)/\sqrt{5}$ on the equatorial plane, and asymptotes $z = \pm\sqrt{5}R$, so that $\mathrm{Pr}(\mathscr{B}^-)$ coincides with the z-axis. In the top panels of Fig. 4, the red line shows $\mathscr{B}^0$ for three representative values of s. Moreover, the radial derivative of the first of equation (27) shows that $D < 0$ over the whole space, and $D = 0$ for $R = 0$, i.e. $\mathscr{D}^0$ coincides with the z-axis; therefore, $\mathrm{Pr}(\mathscr{D}^-)$ coincides with the z-axis, and $\mathscr{D}^+$ is empty. Finally, from the second of equation (13), we get

$$
\mathscr{C}^- = \Big\{ (R, z) : \ 2sR^4 + (s + \zeta)^2(2s + 5\zeta)R^2 -
$$
$$
(s + \zeta)^4\zeta < 0 \Big\}.
\tag{29}
$$

The biquadratic in R above has a positive discriminant, and a permanence and a variation of signs in the coefficients: it follows that $\mathscr{C}^-$ is the portion of the (R, z)-plane contained between the z-axis and the (positive) square root of the (positive) solution of the biquadratic. We do not report here the expression for $\mathscr{C}^0$, which however can be determined without difficulty; $\mathrm{Pr}(\mathscr{C}^-)$ coincides with the z-axis. In the top panels of Fig. 4, the green line shows $\mathscr{C}^0$ for three representative values of s. Again from Fig. 4, it is apparent that $\mathscr{B}^- \subseteq \mathscr{C}^+$ and $\mathscr{C}^- \subseteq \mathscr{B}^+$, as expected from the general discussion in Section 4; notice also how the separation between $\mathscr{B}^-$ and $\mathscr{C}^-$ (i.e. the region $\mathscr{B}^+ \cap \mathscr{C}^+$) becomes larger as s increases. Moreover, in the spherical
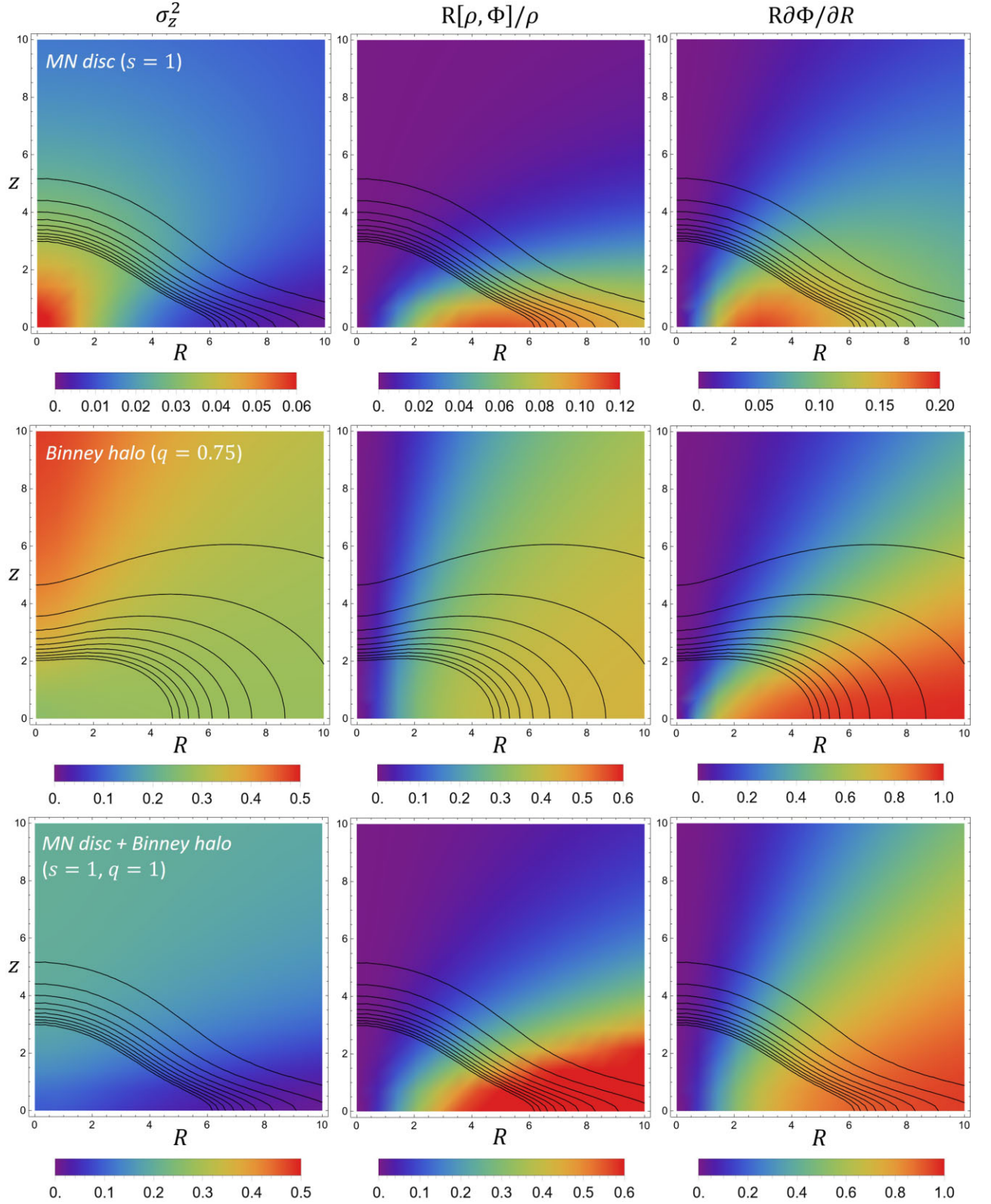
Figure 3. Maps in the (R, z)-plane of σ_z^2 (left column), $R[\rho, \Phi]/\rho$ (central column), and $R\partial\Phi/\partial R$ (right column) for the MN disc with $s = 1$ (top row), for the Binney logarithmic halo with $q = 0.75$ (central row), and for the MN stellar disc ($s = 1$) in a dominant ($\Phi = \Phi_h$) and spherical ($q = 1$) Binney logarithmic dark matter halo with $b_h = 2$. The fields are in units of v_h^2 for the Binney halo, and of GM_*/b_* for the other two models. Black solid lines show equally spaced isodensity contours.
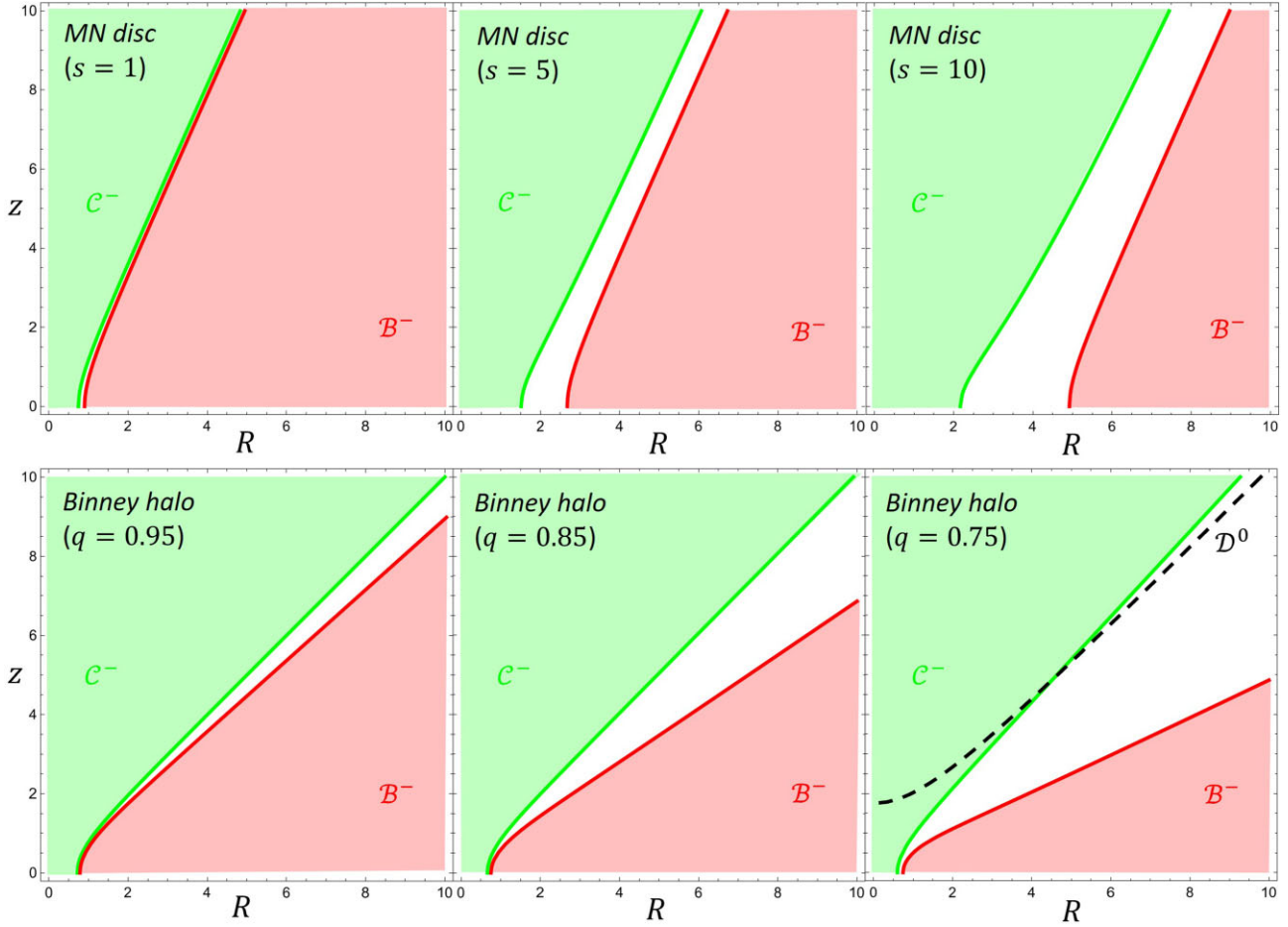
Figure 4. The ansatz-independent regions $\mathscr{B}$, $\mathscr{C}$, and $\mathscr{D}$ of the MN disc (top panels) for different values of s, and of the Binney logarithmic halo (bottom panels) for different values of q; both models become flatter from left to right. Red and green areas correspond to the $\mathscr{B}^-$ and $\mathscr{C}^-$ regions, respectively, while heavy red and green lines are the $\mathscr{B}^0$ and $\mathscr{C}^0$ sets. Except for the Binney model with $q = 0.75$, where $\mathscr{D}^-$ lies below the $\mathscr{D}^0$ line (dashed), for all the other cases $\mathscr{D}^-$ fully covers the (R, z)-plane, with $\mathscr{D}^0$ coinciding with the z-axis. For all models, $\mathrm{Pr}(\mathscr{B}^-)$ and $\mathrm{Pr}(\mathscr{C}^-)$ coincide with the z-axis, and as $[\rho, \Phi] \geq 0$ everywhere, from Theorem B.2, we have $\mathscr{B}^- \cap \mathscr{C}^+ = \mathscr{B}^-$ and $\mathscr{C}^- \cap \mathscr{B}^+ = \mathscr{C}^-$.

case $(s = 0)$ we would obtain $\mathscr{B}^0 = \mathscr{C}^0$, $\mathscr{B}^- = \mathscr{C}^+$ and $\mathscr{B}^+ = \mathscr{C}^-$.

We now determine the constraints on $b(z)$ for the positivity of $\overline{v_\varphi^2}$, Δ_R, and Δ. Remarkably, all the computations in equations (19), (21), (23), and (24) can be carried out explicitly, and we obtain

$$b_M(z) = \frac{6}{5} + \frac{14s + 4\sqrt{s(6s + 15\zeta)}}{25\zeta}, \tag{30}$$

$$b_0(z) = 1 + \frac{s}{3\zeta}, \tag{31}$$

$$b_1(z) = 1, \quad b_2(z) = 1 + \frac{(14 + 4\sqrt{6})s}{25\zeta}. \tag{32}$$

In the top left panel of Fig. 5, we show the four functions for $s = 1$, where the chain of inequalities in equation (25) is apparent, considering that for the MN disc $\mathrm{Pr}(\mathscr{B}^-)$ and $\mathrm{Pr}(\mathscr{C}^-)$ both coincide with the z-axis. If one restricts to b functions independent of z, we have

$$1 = b_1 = b_0 = b_2 < b_M = \frac{6}{5}, \tag{33}$$

independent of s: in particular, this holds for the spherical case (the Plummer sphere).

Fig. 6 illustrates the behaviour of $\overline{v_\varphi^2}$, Δ_R and Δ for the MN disc with $s = 1$, and for three values of b, i.e. $b = 0.5, 1, 2$. The adopted values map three different kinematical configurations, as can be seen from equation (33). For $b = 0.5$, $\overline{v_\varphi^2}$ and Δ_R are everywhere positive, while Δ is expected to be negative over some region in $\mathscr{B}^+ \cap \mathscr{C}^- = \mathscr{C}^-$, being $0.5 < b_1$, and positive over $\mathscr{B}^- \cap \mathscr{C}^+ = \mathscr{B}^-$, being $0.5 < b_2$. This is nicely confirmed by the three left panels in Fig. 6, where white regions indicate negative values of the fields. The three central panels correspond to $b = 1$, i.e. to the two-integral solutions (see also the three top panels in Fig. 3). The fields in this case are everywhere positive, in agreement with the general discussion and equation (33). Note how the increase of b from 0.5 to 1 produces the expected changes summarized in Fig. 2, i.e. $\overline{v_\varphi^2}$ decreases over $\mathscr{B}^-$ and increases over $\mathscr{B}^+$, Δ_R decreases everywhere being $\mathscr{D}^-$ for this model coincident with the (R, z)-plane, and Δ behaves qualitatively as $\overline{v_\varphi^2}$, becoming non-negative over $\mathscr{C}^-$ because $1 = b_1$. Finally, the three right panels of Fig. 6 correspond to the unphysical model with $b > b_M$, and a large region in the $\overline{v_\varphi^2}$ map becomes white: increasing further b would increase the size of the white region up to the whole $\mathscr{B}^-$. However, $\overline{v_\varphi^2}$ continues to increase in $\mathscr{B}^+$. As $2 > b_0$, Δ_R is now negative over a large portion of the (R, z)-plane and, increasing further b, Δ_R would become negative everywhere.
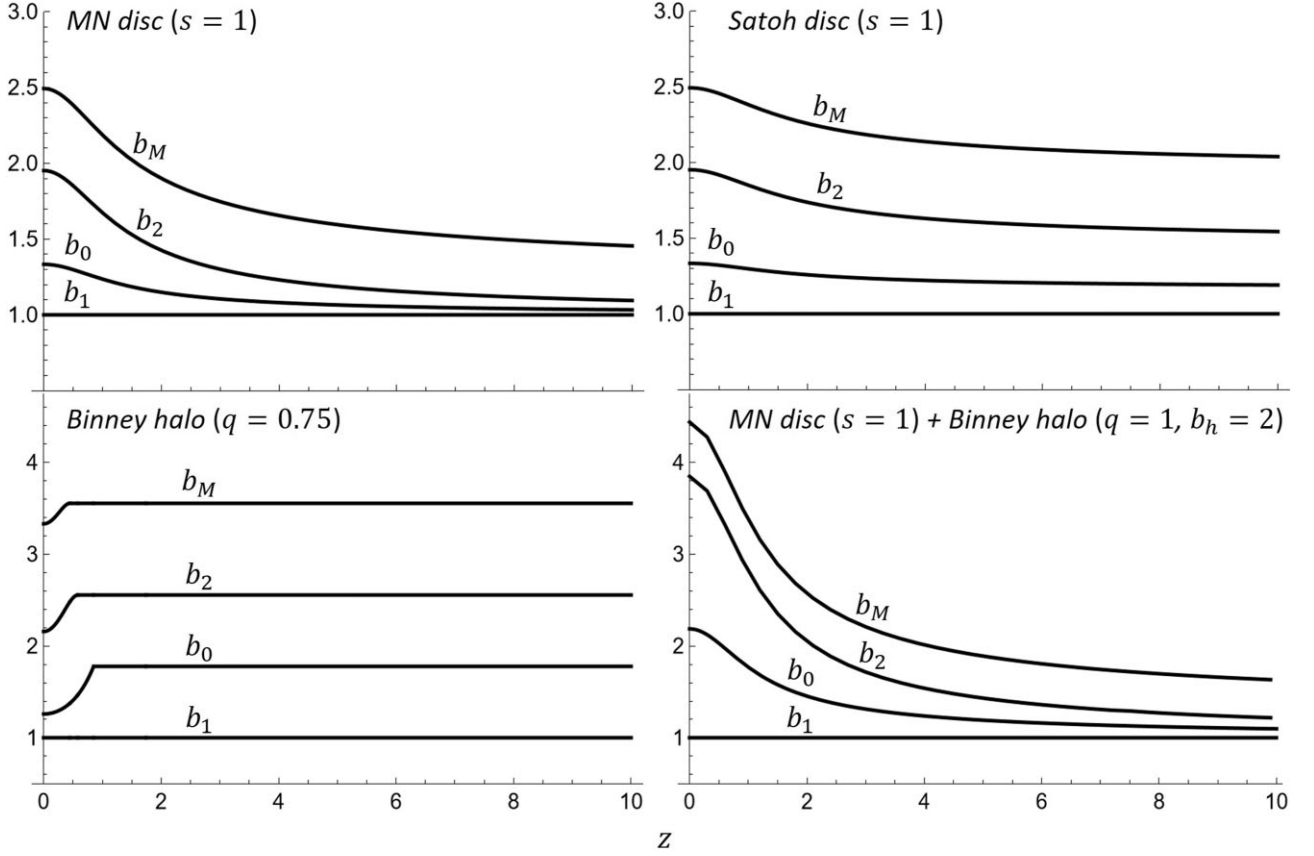
Figure 5. Profiles of $b_1(z)$, $b_0(z)$, $b_2(z)$, and $b_M(z)$ for the MN disc with $s = 1$ (top-left panel), the Satoh disc with $s = 1$ (top-right panel), the Binney logarithmic halo with $q = 0.75$ (bottom-left panel), and the two-component MN disc with $s = 1$ in a dominant ($\Phi = \Phi_h$), spherical ($q = 1$) Binney logarithmic halo with $b_h = 2$ (bottom-right panel). The z-values are normalized to b_h for the Binney model, and to b_* for the other models. Because for these models $[\rho, \Phi] \geq 0$ everywhere, it follows that $b_1(z) \leq b_2(z) \leq b_0(z) \leq b_M(z)$ for all z, as discussed in Section 4.

Finally, the negative region of Δ has now switched to the $\mathscr{B}^-$ region, being $2 > b_2$. Interestingly, the shape and the position of the white region of $\overline{v_\varphi^2}$ resemble those where the numerically evaluated $\overline{v_\varphi^2}$ for the similar model of the Satoh disc with $b = 4/3$ (Cappellari 2020, fig. 10) goes to zero.

5.2 The Satoh disc

The potential–density pair of the Satoh (1980) disc of total mass M_*, and scale lengths a_* and b_*, can be written as

$$
\begin{cases}
\Phi_* = -\dfrac{GM_*}{b_* \xi}, \quad \xi \equiv \sqrt{R^2 + (s + \zeta)^2 - 1}, \\[2ex]
\rho_* = \dfrac{M_*}{b_*^3} \dfrac{s\xi^2 + 3s\zeta(s + 2\zeta)}{4\pi \zeta^3 \xi^5},
\end{cases}
\tag{34}
$$

where again $\zeta \equiv \sqrt{1 + z^2}$, $s \equiv a_*/b_*$ measures the flattening of the disc, and all lengths are assumed to be normalized to $b_* \neq 0$ as throughout the Section. Notice that, at variance with the MN model, the spherical limit of the Satoh model ($s = 0$) reduces to the point mass case of no practical interest. From equations (2) and (3), one has

$$
\rho_* \sigma_z^2 = \frac{GM_*^2}{b_*^4} \frac{s(s + 2\zeta)}{8\pi \zeta^2 \xi^6}, \quad [\rho_*, \Phi_*] = \frac{GM_*^2}{b_*^5} \frac{sR}{4\pi \zeta^3 \xi^6}.
\tag{35}
$$

Similarly to the MN disc, $[\rho_*, \Phi_*] \geq 0$ everywhere, and also the maps of σ_z^2, $[\rho_*, \Phi]$ and $R\partial\Phi/\partial R$ are very similar to those of the MN model in Fig. 3, and thus are not shown.

The $\mathscr{B}$, $\mathscr{C}$ and $\mathscr{D}$ regions can be determined analytically. In particular, we have

$$
\mathscr{B}^- = \left\{ (R, z) : 5R^2 - (s + \zeta)^2 + 1 > 0 \right\},
\tag{36}
$$

so that $\mathscr{B}^-$ is the portion of the (R, z)-plane to the right of the curve $\mathscr{B}^0$ with vertex coordinates $z = 0$ and $R = \sqrt{s(s + 2)/5}$, and asymptotes $z = \pm\sqrt{5}R$; $\mathrm{Pr}(\mathscr{B}^-)$ coincides with the z-axis. The radial derivative of the first of equation (35) shows that $D < 0$ everywhere, except for the z-axis, where $D = 0$; therefore, as for the MN disc, $\mathrm{Pr}(\mathscr{D}^-)$ coincides with the z-axis, and the set $\mathscr{D}^+$ is empty. Finally, from the second of equation (13),

$$
\mathscr{C}^- = \Big\{ (R, z) : \quad 2R^4 + R^2(12\zeta^2 + 9s\zeta + 2s^2 - 2) \\
- (\zeta + s + 1)(\zeta + s - 1)(s + 2\zeta)\zeta < 0 \Big\},
\tag{37}
$$

and again, similarly to the MN disc, the resulting expression is a biquadratic with two real solutions. From the fact that $\zeta \geq 1$, the coefficients present a permanence and a variation of their sign: therefore, $\mathscr{C}^-$ is the region between the z-axis and the (positive) square root of the (positive) solution of the biquadratic. The explicit expression of $\mathscr{C}^0$ can be obtained without difficulty; we just notice that, as for the MN disc, $\mathrm{Pr}(\mathscr{C}^-)$ coincides with the z-axis. Again, all
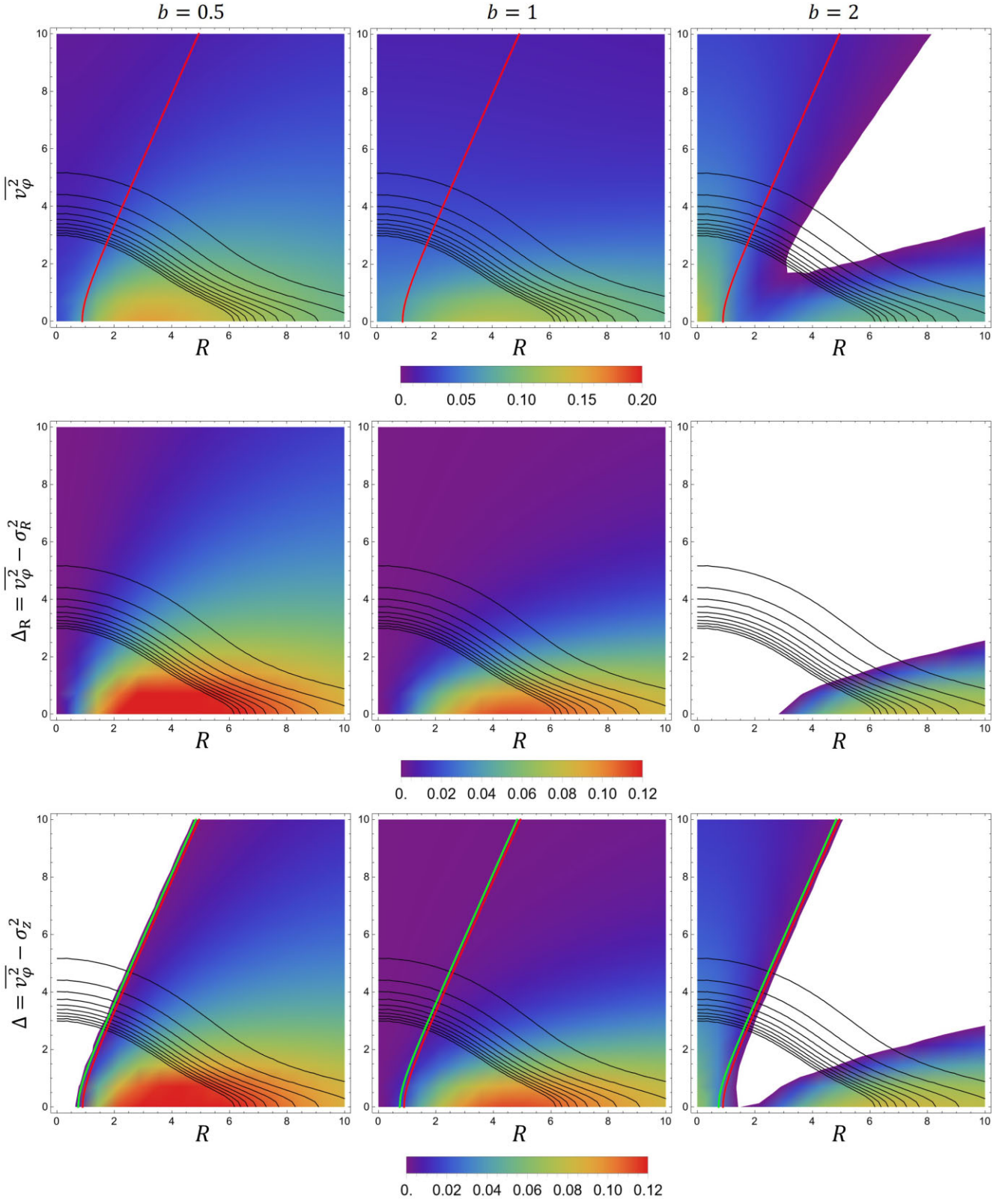
Figure 6. Maps in the (R, z)-plane of $\overline{v_\varphi^2}$ (top row), Δ_R (central row), and Δ (bottom row) in units of GM_*/b_* for the MN disc with $s = 1$ and constant $b = 0.5$ (left column), $b = 1$ (central column), and $b = 2$ (right column). Black solid lines show equally spaced isodensity contours of the stellar distribution. The red and green lines show, respectively, the $\mathscr{B}^0$ and $\mathscr{C}^0$ curves, while $\mathscr{D}^0$ coincides with the z-axis. White regions correspond to negative values of the fields.

the results summarized in Section 4 about the relative position of the regions apply, i.e. $\mathscr{B}^- \subseteq \mathscr{D}^-$, and $\mathscr{B}^- \cap \mathscr{C}^+ = \mathscr{B}^-$, $\mathscr{B}^+ \cap \mathscr{C}^- = \mathscr{C}^-$.

The limitations on $b(z)$ for the positivity of $\overline{v_\varphi^2}$, Δ_R and Δ can all be obtained analytically. From equations (19), (21), (23), and (24),

$$b_{\rm M}(z) = \frac{6}{5} + \frac{14\zeta_*^2 + 2\zeta_*\sqrt{24\zeta_*^2 + 60\zeta(s+2\zeta)}}{25\zeta(s+2\zeta)}, \tag{38}$$

$$b_0(z) = 1 + \frac{\zeta_*^2}{3\zeta(s+2\zeta)}, \tag{39}$$

$$b_1(z) = 1, \quad b_2(z) = 1 + \frac{(14 + 4\sqrt{6})\zeta_*^2}{25\zeta(s+2\zeta)}, \tag{40}$$

where $\zeta_* \equiv \sqrt{(s+\zeta)^2 - 1}$. In the top right panel of Fig. 5, we show the four functions above for $s = 1$; again, they fulfil the inequalities in equation (25), considering that ${\rm Pr}(\mathscr{B}^-)$ and ${\rm Pr}(\mathscr{C}^-)$ both coincide with the z-axis. For a spatially constant b, we have

$$b_1 = 1 < b_0 = \frac{7}{6} < b_2 = \frac{32 + 2\sqrt{6}}{25} < b_{\rm M} = \frac{49}{25}, \tag{41}$$

independently of s.

We do not show the analogous of Fig. 6, due to the close similarity, for sufficiently flat models, with the MN case, so that all comments made for the MN disc apply. The only noticeable difference is that now $b_1 \neq b_0 \neq b_2$, while for the MN disc they are the same [see equation (33)].

5.3 The Binney logarithmic halo

The potential–density pair of the Binney logarithmic halo (BT08) of asymptotic circular velocity $v_{\rm h}$, scale length $b_{\rm h}$, and potential flattening q is

$$\begin{cases} \Phi_{\rm h} = \dfrac{v_{\rm h}^2}{2} \ln\left(1 + R^2 + \dfrac{z^2}{q^2}\right), \\[3mm] \rho_{\rm h} = \dfrac{v_{\rm h}^2}{4\pi G b_{\rm h}^2} \dfrac{1 + 2q^2 + R^2 + \left(2 - q^{-2}\right)z^2}{q^2\left(1 + R^2 + q^{-2}z^2\right)^2}, \end{cases} \tag{42}$$

where throughout this Section the lengths are assumed normalized to $b_{\rm h} \neq 0$. As well known, for $q < 1/\sqrt{2}$, $\rho_{\rm h}$ becomes negative on the z-axis. The dynamical properties of this model are given by Evans (1993) (see also Evans 1994 and Evans & de Zeeuw 1994 for the properties of the larger family of the so-called power-law models); here we just use equations (2) and (3) to obtain

$$\begin{cases} \rho_{\rm h}\sigma_z^2 = \dfrac{v_{\rm h}^4}{G b_{\rm h}^2} \dfrac{q^4 R^2 + (2q^2 - 1)z^2 + 2q^4}{8\pi(q^2 R^2 + z^2 + q^2)^2}, \\[3mm] [\rho_{\rm h}, \Phi_{\rm h}] = \dfrac{v_{\rm h}^4}{G b_{\rm h}^3} \dfrac{q^2(1 - q^2)R}{4\pi(q^2 R^2 + z^2 + q^2)^2}, \end{cases} \tag{43}$$

so that $\sigma_z^2 \geq 0$ for $q \geq 1/\sqrt{2}$. Moreover, $[\rho_{\rm h}, \Phi_{\rm h}] \geq 0$ for $1/\sqrt{2} \leq q < 1$, it vanishes for $q = 1$ (the spherical limit), and it is ≤ 0 for $q > 1$. We finally notice that, in the two-integral case,

$$\rho_{\rm h}\overline{v_\varphi^2} = \frac{v_{\rm h}^4}{G b_{\rm h}^2} \frac{q^2(2 - q^2)R^2 + (2q^2 - 1)z^2 - 2q^4}{8\pi(q^2 R^2 + z^2 + q^2)^2}, \tag{44}$$

showing that $\overline{v_\varphi^2}$ becomes negative for $q > \sqrt{2}$, and the models are hence inconsistent. Actually, Evans (1993) proved that the two-integral DF becomes negative for $q \gtrsim 1.08$ so that models with

$1.08 \lesssim q \leq \sqrt{2}$ do not exist[2] although they have non-negative σ_z^2 and $\overline{v_\varphi^2}$. From now on, we consider models with $1/\sqrt{2} \leq q \leq 1$, so that $[\rho_{\rm h}, \Phi_{\rm h}] \geq 0$ everywhere: in the central panels of Fig. 3, the 2D maps of σ_z^2, $[\rho_{\rm h}, \Phi_{\rm h}]$, and $R\partial\Phi/\partial R$ are shown for $q = 0.75$.

As for the two previous models, the $\mathscr{B}$, $\mathscr{C}$ and $\mathscr{D}$ regions can be determined in a fully analytical way. We notice however that for $q \simeq 1$ the Binney halo is qualitatively different from a disc, resembling a spheroid; therefore, we expect some important differences compared to the previously discussed cases. From equation (43), we have

$$\mathscr{B}^- = \Big\{(R, z): \quad q^6 R^4 + 3q^2(q^2 z^2 - z^2 + q^4)R^2$$
$$- (q^2 + z^2)(2q^2 z^2 - z^2 + 2q^4) > 0\Big\}. \tag{45}$$

With some work, it can be proved that the discriminant of the biquadratic is strictly positive independently of q; moreover, for $q \geq 1/\sqrt{2}$, the last term in equation (45) is negative, so that a permanence and a variation of the sign of its coefficients are present. We conclude that $\mathscr{B}^0$ is the (positive) square root of the (positive) solution, and $\mathscr{B}^-$ is the region of the (R, z)-plane to the right of $\mathscr{B}^0$. As for the previous models, ${\rm Pr}(\mathscr{B}^-)$ coincides with the z-axis; for simplicity, we do not report the explicit expression of $\mathscr{B}^0$ here, but we show it as the red line in the bottom panels of Fig. 4, for three representative values of q. The properties of the $\mathscr{D}$ region are more complicated compared to the previous cases: in fact, while for $q \geq \sqrt{2/3}$, $D < 0$ everywhere (vanishing on the z-axis) and thus $\mathscr{D}^-$ fully covers the (R, z)-plane, for $q < \sqrt{2/3}$

$$\mathscr{D}^- = \left\{(R, z): z - \frac{q^2\sqrt{3 + R^2}}{\sqrt{2 - 3q^2}} < 0\right\}, \tag{46}$$

and the $\mathscr{D}^+$ region now exists: for example, in the bottom right panel of Fig. 4, the dashed line shows $\mathscr{D}^0$ for $q = 0.75$, and $\mathscr{D}^+$ is the part of the plane above it. Notice how, independently of q, ${\rm Pr}(\mathscr{D}^-)$ coincides with the z-axis. Finally, from equation (13),

$$\mathscr{C}^- = \Big\{(R, z): q^4(2 - q^2)R^4 + q^2(q^2 z^2 - z^2 + q^4$$
$$+ 2q^2)R^2 - (q^2 + z^2)(2q^2 z^2 - z^2 + 2q^4) < 0\Big\}, \tag{47}$$

where, in the considered range of $1/\sqrt{2} \leq q \leq 1$, the discriminant of the biquadratic is positive, and the coefficients present a permanence and a variation of the sign. Therefore, $\mathscr{C}^0$ is the (positive) square root of the (positive) solution, and $\mathscr{C}^-$ is the region between the z-axis and $\mathscr{C}^0$; ${\rm Pr}(\mathscr{C}^-)$ coincides with the z-axis. In the bottom panels of Fig. 4, the green line shows $\mathscr{C}^0$ for three representative values of q. It is also apparent how $\mathscr{B}^- \subseteq \mathscr{D}^-$, $\mathscr{B}^- \cap \mathscr{C}^+ = \mathscr{B}^-$ and $\mathscr{B}^+ \cap \mathscr{C}^- = \mathscr{C}^-$, as expected from the general discussion; similarly to the MN model, notice that the $\mathscr{B}^+ \cap \mathscr{C}^+$ region becomes larger as q decreases, i.e. for more flattened systems. Again, in the spherical case ($q = 1$) we would obtain $\mathscr{B}^0 = \mathscr{C}^0$, $\mathscr{B}^- = \mathscr{C}^+$ and $\mathscr{B}^+ = \mathscr{C}^-$.

We now determine the constraints on $b(z)$ from the request of positivity for $\overline{v_\varphi^2}$, Δ_R and Δ. From equation (19), with $1/\sqrt{2} \leq q \leq 1$,

$$b_{\rm M}(z) = \frac{2}{q^2}, \quad z \geq z_{\rm M}(q) \equiv \frac{q^2\sqrt{1 - q^2}}{\sqrt{q^4 - 2q^2 + 3/2}}, \tag{48}$$

---

[2]This case exemplifies that $\sigma_z^2 \geq 0$ and $\overline{v_\varphi^2} \geq 0$ are only *necessary* conditions for the model consistency, while $\sigma_z^2 < 0$ or $\overline{v_\varphi^2} < 0$ are *sufficient* to prove the model inconsistency.

while for $z \leq z_M$, $b_M(z)$ is a complicated function monotonically decreasing from $2/q^2$ to the minimum

$$b_M(0) = \frac{14 + 12q^2 + 8\sqrt{2 + q^2 - 2q^4}}{17q^2}, \tag{49}$$

reached on the equatorial plane; in the spherical case ($q = 1$), $b_M(z) = 2$ for all z. From equation (21),

$$b_0(z) = \frac{1}{q^2}, \quad z \geq z_0(q) \equiv \frac{q^2}{\sqrt{1 - q^2}}, \tag{50}$$

and for $z \leq z_0$, $b_0(z)$ is a complicated function monotonically decreasing from $1/q^2$ to the minimum

$$b_0(0) = \frac{2}{3} + \frac{1}{3q^2}, \tag{51}$$

reached again on the equatorial plane; in the spherical case, $b_0(z) = 1$ for all z, as expected from the general discussion. Finally, from equations (23) and (24), $b_1(z) = 1$, and

$$b_2(z) = \frac{2}{q^2} - 1, \quad z \geq z_2(q) \equiv \frac{\sqrt{2}q^2}{\sqrt{3 - 2q^2}}, \tag{52}$$

while for $z \leq z_2$, $b_2(z)$ is again a complicated function which decreases monotonically, reaching its minimum

$$b_2(0) = \frac{14 + 8\sqrt{2} + (3 - 8\sqrt{2})q^2}{17q^2}, \tag{53}$$

on the equatorial plane; in the spherical case, $b_2(z) = 1$. In the bottom-left panel of Fig. 5, we show the four $b(z)$ functions described above for the representative case of $q = 0.75$: the chain of inequalities in equation (25) is apparent, even though the profiles qualitatively differ from those of the two disc cases. In particular, if one restricts to the constant b case, we have $b_1 = 1 \leq b_0(0) \leq b_2(0) < b_M(0)$.

Fig. 7 shows the 2D maps of $\overline{v_\varphi^2}$, Δ_R and Δ for the Binney logarithmic halo with $q = 0.75$ and for three values of b, i.e. $b = 0.5$, 1, 3.75. The adopted values of b allow to illustrate three representative kinematical behaviours. When $b = 0.5$, we expect $\overline{v_\varphi^2}$ and Δ_R to be everywhere positive, while a negative Δ is expected over some region in $\mathscr{C}^-$, being $0.5 < b_1 = 1$, and positive over $\mathscr{B}^-$, being $0.5 < b_2 \simeq 2.16$. This is nicely confirmed by the three left panels, where white regions indicate negative values. The three central panels correspond to $b = 1$, i.e. to the two-integral solutions, and complement the three middle panels in Fig. 3. The fields for $b = 1$ case are everywhere positive, in agreement with the general discussion and equations (49), (51) and (53). The increase of b from 0.5 to 1 produces, as expected, that $\overline{v_\varphi^2}$ decreases over $\mathscr{B}^-$ and increases over $\mathscr{B}^+$, Δ_R decreases over $\mathscr{D}^-$ and increases over $\mathscr{D}^+$, and Δ behaves qualitatively as $\overline{v_\varphi^2}$, becoming non-negative over $\mathscr{C}^-$ because $1 = b_1$. Finally, the three right panels correspond to the unphysical model with $b > b_M \simeq 3.33$, and a portion of $\mathscr{B}^-$ is already white; compared to the disc models, this region is more confined near the equatorial plane. Increasing further b would extend the white region to cover the whole $\mathscr{B}^-$, while $\overline{v_\varphi^2}$ would continue increasing in $\mathscr{B}^+$. As $3.75 > b_0 \simeq 1.26$, Δ_R is now negative over a large portion of $\mathscr{D}^-$ and, increasing further b, Δ_R would become negative over the whole $\mathscr{D}^-$ region, i.e. below the yellow line. At variance with discs, however, Δ_R would remain positive and increase above the line. Finally, the negative region of Δ has now switched to the $\mathscr{B}^-$ region, being $3.75 > b_2$.

6 A TWO-COMPONENT MODEL: THE MIYAMOTO & NAGAI DISC IN A BINNEY LOGARITHMIC HALO

We now study whether and how the presence of a dark matter (DM) halo changes the conclusions obtained for one-component models. In particular, we consider the two-component model made by a stellar MN disc embedded in a DM Binney logarithmic halo. We adopt this model because σ_z^2 and the commutator for the stellar distribution can be given in closed form for arbitrary values of s and q (Smet, Posacki & Ciotti 2015, hereafter S15); the resulting expressions are however sufficiently complicated to exclude the possibility of a simple analytical study of the $\mathscr{B}$, $\mathscr{C}$, and $\mathscr{D}$ regions, which are determined in a numerical way starting from the analytical formulae in S15.

By using the normalizations adopted for the MN model, i.e. b_* for lengths and GM_*/b_* for potentials, the dimensionless total potential is

$$\Phi = \Phi_* + \mathscr{R}\Phi_h, \quad \mathscr{R} \equiv \frac{v_h^2 b_*}{GM_*}, \tag{54}$$

in which $\Phi_* = -1/\xi$, as given in equation (26), and from equation (42) the dimensionless halo potential is

$$\Phi_h = \frac{1}{2} \ln \left(1 + \frac{R^2}{b_h^2} + \frac{z^2}{q^2 b_h^2} \right), \tag{55}$$

where b_h is the scale length of the halo now in units of b_*, i.e. a dimensionless parameter. For $\mathscr{R} = 0$, the model reduces to the self-gravitating MN disc, while for $\mathscr{R} \gg 1$ we obtain the 'halo-dominated' case, in practice equivalent to considering $\Phi = \Phi_h$ in the JEs. Notice that, at sufficiently large $r = \sqrt{R^2 + z^2}$, the model is always halo-dominated, independently of the value of $\mathscr{R}$.

In the two-integral case, σ_z^2 of the stellar distribution can be obtained by adding equations (10) and (17) of S15, while $[\rho_*, \Phi]$ can be obtained from equation (27) of S15. It can be shown that, while $\sigma_z^2 \geq 0$ regardless of the model parameters, the sign of $[\rho_*, \Phi]$ depends on the value of q, and if $q < 1$, there are regions at large r where $[\rho_*, \Phi] < 0$. Instead, if $q \geq 1$, then $[\rho_*, \Phi] \geq 0$ everywhere. We notice that an asymptotic analysis of the solutions of the JEs shows that, independently of s and $\mathscr{R}$, $\overline{v_\varphi^2}$ becomes negative at large distances from the origin for $q \lesssim 0.85$; instead, for $q \gtrsim 0.85$, $\overline{v_\varphi^2} \geq 0$ everywhere.

As we expect that the halo-dominated models are the most different compared to the one-component MN disc, in the following we focus on these models, and for simplicity, we consider a spherical ($q = 1$) halo. In the three bottom panels of Fig. 3, we show the maps of σ_z^2, $[\rho_*, \Phi]$ and $R\partial\Phi/\partial R$ for a halo-dominated MN disc with $s = 1$, and $b_h = 2$. By comparison with the MN panels in the figure, it is apparent that the main effect of the halo is to produce an increase of σ_z^2, and of the commutator at large radii near the equatorial plane, as expected given the flat rotation curve of the halo at large radii. Instead, in the more central regions, the self-gravitating effects of the disc are not visible because the gravitational field of the disc is neglected everywhere in the presented model.

However, even though the gravitational potential is dominated by the halo, the disc density distribution enters the B, C, and D functions, so we expect that the $\mathscr{B}$, $\mathscr{C}$, and $\mathscr{D}$ regions, whose determination now must be carried out numerically, are not coincident with those of the Binney halo (see Section 5.3). Indeed, now the $\mathscr{B}$ and $\mathscr{C}$ regions are more similar to those of the MN disc, and $\mathscr{D}^-$ coincides with the (R, z)-plane, with $D = 0$ on the z-axis.
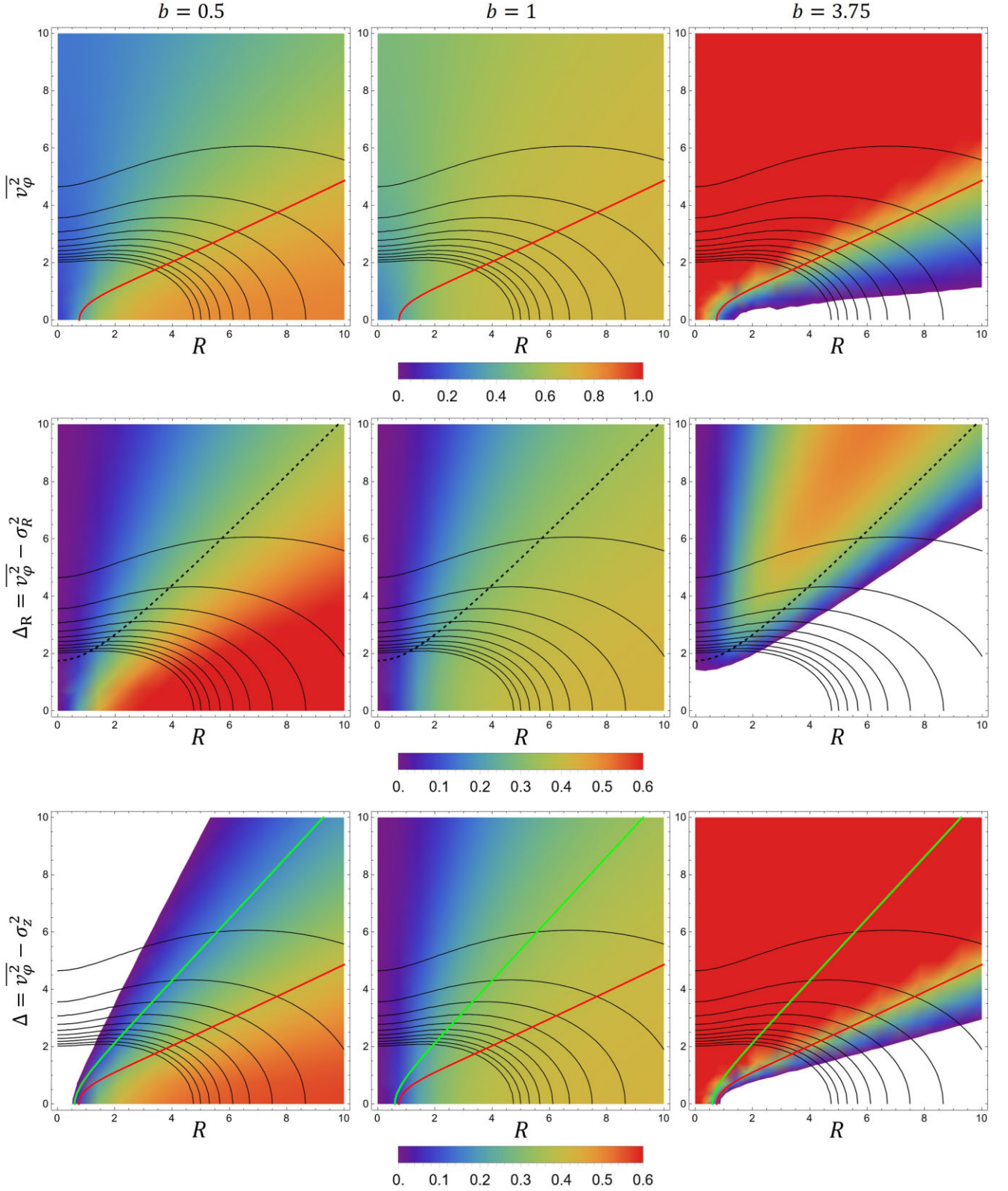
Figure 7. Maps in the (R, z)-plane of $\overline{v_\varphi^2}$ (top row), Δ_R (central row), and Δ (bottom row) in units of v_h^2, for the Binney logarithmic halo with $q = 0.75$ and constant $b = 0.5$ (left column), $b = 1$ (central column), and $b = 2$ (right column). Black solid lines show equally spaced isodensity contours of the stellar distribution. The red, green, and black dashed lines show, respectively, the $\mathscr{B}^0$, $\mathscr{C}^0$, and $\mathscr{D}^0$ curves. White regions correspond to negative values of the fields.

Due to the numerical determination of the $\mathscr{B}$, $\mathscr{C}$ and $\mathscr{D}$ regions, also the various constraints on the b values had to be found numerically. In

the bottom-right panel of Fig. 5, we show the four $b(z)$ constraints for the halo-dominated model with $q = 1$, $s = 1$ and $b_h = 2$. Reassuringly,
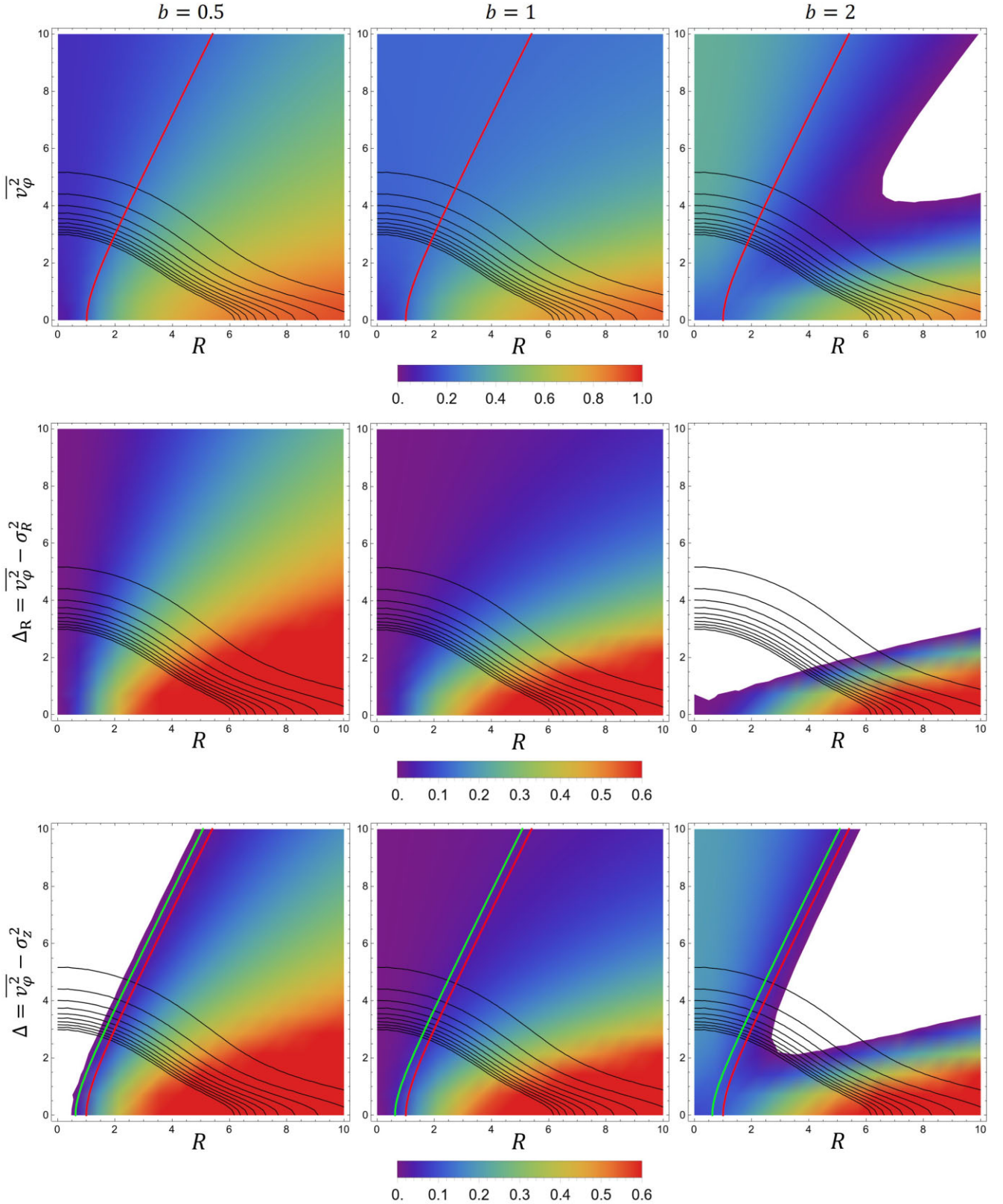
Figure 8. Maps in the (R, z)-plane of $\overline{v_\varphi^2}$ (top row), Δ_R (central row), and Δ (bottom row) in units of GM_*/b_* for the MN disc with $s = 1$ in a dominant ($\Phi = \Phi_h$), spherical ($q = 1$) Binney logarithmic halo with $b_h = 2$, and constant $b = 0.5$ (left column), $b = 1$ (central column), and $b = 2$ (right column). Black solid lines show equally spaced isodensity contours of the stellar distribution. The red and green lines show, respectively, the $\mathscr{B}^0$ and $\mathscr{C}^0$ curves. White regions correspond to negative values of the fields.

they obey the inequality in equation (25), being the commutator positive everywhere. For the constant b case, they can be obtained analytically through an asymptotic analysis, and we found that $b_1 = b_0 = b_2 = 1$, and $b_M = 5/4$.

Fig. 8 shows the 2D maps of $\overline{v_\varphi^2}$, Δ_R and Δ for the same $q = 1$, $s = 1$ and $b_h = 2$, and for $b = 0.5, 1, 2$ (as in Fig. 6 for the MN disc). The main result is that the fields are more similar to those of the one-component MN disc in Fig. 6 than to those of the one-component Binney model in Fig. 7, even though the MN disc is halo-dominated. Therefore, we conclude that under the b-ansatz a DM halo does not alter appreciably the qualitative behaviour of the kinematical fields of the disc, even when the halo is very massive.

7 SUMMARY AND CONCLUSIONS

Unless a specific functional form of the phase-space DF is assumed, the JEs do not form a closed system of equations, and to solve them a choice must be made for the link between the velocity moments. In this work, we considered the JEs of axisymmetric systems with three unknowns (σ_z^2, σ_R^2, and $\overline{v_\varphi^2}$), and focused on the choice of $\sigma_R^2 = b(R, z)\sigma_z^2$ (the 'b-ansatz', where b is a positive function), introduced in Cappellari (2008) and widely used in the dynamical modelling of stellar systems. After recalling the JEs in cylindrical coordinates, and the expressions for the ansatz-independent quantities σ_z^2 and $[\rho_*, \Phi]$, and the associated functions B, C, and D defined over the (R, z)-plane, we investigated the behaviour of the kinematical quantities that depend on b as follows:

(i) We first gave the general expressions, as a function of b and of the ansatz-independent quantities, for $\overline{v_\varphi^2}$ and the related functions $\Delta = \overline{v_\varphi^2} - \sigma_z^2$ and $\Delta_R = \overline{v_\varphi^2} - \sigma_R^2$, which enter the Satoh (1980) decomposition of $\overline{v_\varphi^2}$ to derive the ordered rotational velocity $\overline{v_\varphi}$. These general expressions are fundamental to investigate the positivity of $\overline{v_\varphi^2}$, required for the model consistency, and of Δ and Δ_R, necessary for the Satoh (1980) decomposition and its variants. These general expressions also allow to predict, before solving the JEs, the trends of $\overline{v_\varphi^2}$, Δ and Δ_R as a function of b throughout the galaxy, thus avoiding a time-consuming numerical exploration of the parameter space in the modelling.

(ii) For systems with $\partial\Phi/\partial R \geq 0$ everywhere (the common situation), and $b = b(z)$, we discussed the positivity problem in full generality: we first showed how to determine the ansatz-independent regions of the (R, z)-plane where negativity is possible, i.e. $\mathcal{B}^-$ for $\overline{v_\varphi^2}$, $\mathcal{D}^-$ for Δ_R and a more complicate intersection of $\mathcal{B}^\pm$ and $\mathcal{C}^\pm$ for Δ. Then, we showed how to determine the limiting values of $b(z)$ that guarantee positive kinematical fields over these regions: $b(z) \leq b_M(z)$ for $\overline{v_\varphi^2} \geq 0$, $b(z) \leq b_0(z)$ for $\Delta_R \geq 0$, and $b_1(z) \leq b(z) \leq b_2(z)$ for $\Delta \geq 0$. In the common case of $[\rho_*, \Phi] \geq 0$ everywhere (as for oblate self-gravitating systems), one has $b_1(z) \leq 1$ for $z \in \mathrm{Pr}(\mathcal{C}^-)$, and $1 \leq b_0(z) \leq b_2(z) \leq b_M(z)$ for $z \in \mathrm{Pr}(\mathcal{B}^-)$.

(iii) In particular, for systems with $[\rho_*, \Phi] \geq 0$, we showed that as b increases, in addition to the trivial fact that $\sigma_R^2 = b\sigma_z^2$ increases, $\overline{v_\varphi^2}$ and Δ decrease over $\mathcal{B}^-$ and increase over $\mathcal{B}^+$, and Δ_R decreases over $\mathcal{D}^-$ and increases over $\mathcal{D}^+$.

After the general analysis of the problem and the setup of the procedure to investigate the kinematical properties of a model as a function of b, we illustrated the method with three widely used galaxy models: the Miyamoto & Nagai and Satoh discs, and the Binney logarithmic halo. In doing so, we obtained the following results:

(i) The shape of the $\mathcal{B}^\pm$, $\mathcal{C}^\pm$ and $\mathcal{D}^\pm$ regions and the limits on $b(z)$ can all be obtained analytically. For the two discs, $\mathcal{D}^-$ (the region where $\partial\rho_*\sigma_z^2/\partial R < 0$) coincides with the ($R$, z)-plane, independently of the disc flattening; for the Binney halo, instead, there is a critical value of the potential flattening such that for flatter potentials the region $\mathcal{D}^+$ appears, bounded by a curve containing the z-axis. For all the models, $\mathcal{B}^-$ and $\mathcal{C}^-$ are also bounded by hyperbola-like curves but contain the R-axis. Concerning the limits on $b(z)$, for all the models $\mathrm{Pr}(\mathcal{B}^-) = \mathrm{Pr}(\mathcal{C}^-) = \mathrm{Pr}(\mathcal{D}^-)$ coincide with the z-axis, and $b_1(z) \leq 1 \leq b_0(z) \leq b_2(z) \leq b_M(z)$.

(ii) With the aid of two-dimensional maps, we illustrated how the kinematical fields change over the galaxy by changing b, assumed spatially constant. The results are in agreement with the general considerations, both for their trend with b, and for the regions where they become negative, confirming the utility of the preliminary analysis.

(iii) We finally applied the procedure to the two-component model made by a stellar MN disc embedded in a dominant, spherical dark matter Binney halo; in this case, the investigation has been carried out numerically. The dark halo does not alter appreciably the qualitative trend of the kinematical fields of the stellar disc as a function of b, even when the halo is very massive.

A final comment is worth on the relation between σ_φ^2 and σ_R^2 as a function of b and γ, the other parameter that measures the orbital anisotropy, with positive values corresponding to radial anisotropy, and negative ones to tangential anisotropy [see equations (16) and (17)]. As noticed in Section 3.1, γ is necessarily positive where $\Delta_R < 0$; where $\Delta_R > 0$, instead, γ can be positive ($k^2 > 1$ in the Satoh decomposition) or negative ($k^2 < 1$). Allowing for b and γ as free parameters in the JAM method, the stellar kinematics of regular rotators in the ATLAS^3D survey could be successfully modelled (e.g. Cappellari 2016). It turned out that on average $b > 1$ and $\gamma \approx 0$, within about one effective radius; a limit was also found in the orbital anisotropy, of $\beta = 1 - 1/b \lesssim 0.7\epsilon_{intr}$, where ϵ_{intr} is the intrinsic flattening of the galaxy. This limit had first been found with the Schwarzschild orbit superposition method for the galaxies of the SAURON survey (Cappellari et al. 2007), and thereafter has been often shown in the (V/σ, ϵ), and (λ_R, ϵ) diagrams of larger samples of regular rotators, until those of the MaNGA survey (e.g. Wang et al. 2020). In a recent work, Wang et al. (2021) investigated the origin of this limit: with the JAM modeling, they built mock samples of axisymmetric galaxies with a velocity dispersion ellipsoid appropriate to reproduce the observed fast rotators ($\gamma \approx 0$), and with the mass-follows-light hypothesis. They found an upper limit on β by excluding values producing a negative $\overline{v_\varphi^2}$ over a non-negligible region of the galaxy, clearly an unphysical solution. Our analysis can provide an interpretation for the existence of this limit. In fact, from equation (16), the request of positivity for $\overline{v_\varphi^2}$ with $\gamma \approx 0$ translates into the request of $\Delta_R \gtrsim 0$, and then of $b \lesssim b_0$. Interestingly, for the mass models considered in this work, b_0 increases with the flattening [see equations (31), (39), (50), and (51)], in agreement with the trend shown by the maximum values estimated for β (of $\beta_{max} \sim 0.7\epsilon_{intr}$).

DATA AVAILABILITY

No data sets were generated or analysed in support of this research.

REFERENCES

Barnabè M., Ciotti L., Fraternali F., Sancisi R., 2006, A&A, 446, 61
Bertin G., Varri A. L., 2008, ApJ, 689, 1005
Binney J., 2010, MNRAS, 401, 2318
Binney J., Mamon G. A., 1982, MNRAS, 200, 361
Binney J., Tremaine S., 2008, Galactic Dynamics, 2nd edn. Princeton Univ. Press, Princeton, NJ(BT08)
Binney J., Vasiliev E., 2023, MNRAS, 520, 1832
Cappellari M., 2008, MNRAS, 390, 71
Cappellari M., 2016, ARA&A, 54, 597
Cappellari M., 2020, MNRAS, 494, 4819
Cappellari M. et al., 2007, MNRAS, 379, 418
Cappellari M. et al., 2013, MNRAS, 432, 1862
Ciotti L., 2021, Introduction to Stellar Dynamics. Cambridge Univ. Press, Cambridge (C21)
Ciotti L., Pellegrini S., 1992, MNRAS, 255, 561
Ciotti L., Pellegrini S., 1996, MNRAS, 279, 240
Evans N. W., 1993, MNRAS, 260, 191
Evans N. W., 1994, MNRAS, 267, 333
Evans N. W., de Zeeuw P. T., 1994, MNRAS, 271, 202
King I., 1963, AJ, 68, 282
Kuzmin G., 1956, Astron. Zh., 33, 27
Li H., Li R., Mao S., Xu D., Long R. J., Emsellem E., 2016, MNRAS, 455, 3680
Loubser S. I., Babul A., Hoekstra H., Bahé Y. M., O'Sullivan E., Donahue M., 2020, MNRAS, 496, 1857
Miyamoto M., Nagai R., 1975, PASJ, 27, 533
Negri A., Pellegrini S., Ciotti L., 2013, Mem. Soc. Astron. Ital., 84, 762
Nitschai M. S., Eilers A.-C., Neumayer N., Cappellari M., Rix H.-W., 2021, ApJ, 916, 112
Plummer H. C., 1911, MNRAS, 71, 460
Posti L., Binney J., Nipoti C., Ciotti L., 2015, MNRAS, 447, 3060
Satoh C., 1980, PASJ, 32, 41
Schwarzschild M., 1979, ApJ, 232, 236
Scott N. et al., 2015, MNRAS, 451, 2723
Smet C. O., Posacki S., Ciotti L., 2015, MNRAS, 448, 2921
Statler T. S., 1987, ApJ, 321, 113
Stiavelli M., Bertin G., 1985, MNRAS, 217, 735
Surti T., Romani R. W., Scharwächter J., Peck A., Taylor G. B., 2024, ApJ, 960, 110
Thomas J. et al., 2009, MNRAS, 393, 641
Toomre A., 1963, ApJ, 138, 385
Wang B., Cappellari M., Peng Y., Graham M., 2020, MNRAS, 495, 1958
Wang B., Cappellari M., Peng Y., 2021, MNRAS, 500, L27
Zhu L. et al., 2016, MNRAS, 462, 4001
Zhu K., Lu S., Cappellari M., Li R., Mao S., Gao L., 2023, MNRAS, 522, 6326

APPENDIX A: THE MOST GENERAL $\overline{v_\varphi^2}$ DECOMPOSITION, AND AN ALTERNATIVE ANSATZ FOR THE RADIAL JE

A1 The λ-decomposition for $\overline{v_\varphi^2}$

Once the necessary condition $\overline{v_\varphi^2} \geq 0$ is satisfied by the solution of equation (8), a choice is required to decompose $\overline{v_\varphi^2}$ in its streaming $\overline{v_\varphi}^2$ and dispersion σ_φ^2 components. By construction, the Satoh decomposition presented in Sections 2.1 and 3.1 requires Δ (or Δ_R) ≥ 0. Clearly, if Δ (or Δ_R) is negative over some region of the (R, z)-plane, a generalized Satoh decomposition can be applied just by imposing $k(R, z) = 0$ over this region. However, this decomposition

is quite 'rigid', leading necessarily to $\overline{v_\varphi} = 0$ and $\sigma_\varphi^2 = \overline{v_\varphi^2}$ there. It is therefore useful to provide the most general decomposition of a positive $\overline{v_\varphi^2}$: we refer to this as the λ-decomposition. It is simple to realize that *all* the decompositions are of the form

$$\overline{v_\varphi} = \lambda \sqrt{\overline{v_\varphi^2}} \ , \ \ \sigma_\varphi^2 = (1 - \lambda^2)\overline{v_\varphi^2}, \tag{A1}$$

where in full generality $0 \leq \lambda^2 \ (R, z) \leq 1$, with negative values of λ corresponding to regions of 'counter-rotation'. Two limit cases are possible: $\lambda = 0$ corresponds to no net rotation in the azimuthal direction, and $\lambda^2 = 1$ corresponds to a maximally rotating model. The value of λ corresponding to the isotropic rotator is obtained by imposing $\sigma_\varphi^2 = \sigma_z^2$ from the second of equation (A1), so that

$$\lambda_I^2(R, z) \equiv \frac{\Delta}{\overline{v_\varphi^2}}, \tag{A2}$$

where $\Delta = \overline{v_\varphi^2} - \sigma_z^2 \geq 0$ for isotropy given by the second of equation (1).

Of course, being the λ-decomposition the most general possible, any other decomposition of $\overline{v_\varphi^2}$ must be related to it. For example, if $\Delta \geq 0$ and the Satoh decomposition is hence possible, the following relation between λ and k holds:

$$\lambda = k \sqrt{\frac{\Delta}{\overline{v_\varphi^2}}}. \tag{A3}$$

This shows how, except for the non-rotating case, a spatially constant k does *not* necessarily correspond to a spatially constant λ, and vice versa.

A2 The μ-ansatz for Δ_R

As discussed in Section 3, an ansatz is required to solve the radial JE, and the consequences of assuming the b-ansatz are discussed in this work. We consider here a second family of ansatz ('μ-ansatz') in which priority is given to the relation between Δ_R and the unknown σ_R^2, so that:

$$\Delta_R = \mu\sigma_R^2, \ \ \ \overline{v_\varphi^2} = (1 + \mu)\sigma_R^2, \tag{A4}$$

with the obvious constraint that $\mu(R, z) \geq -1$. Given this choice, it is possible to solve in closed form the radial JE and obtain σ_R^2. In fact, combining equations (8) and (A4) leads to a linear, non-homogeneous differential equation prone to an explicit solution, similar to that for anisotropic spherically symmetric systems (Binney & Mamon 1982; C21). Assuming a vanishing radial 'pressure' at infinity, the solution of the equation reads

$$\rho_*\sigma_R^2 = \int_R^\infty \rho_*(u, z)\frac{\partial\Phi(u, z)}{\partial u}e^{-g(u, R, z)}du, \tag{A5}$$

where

$$g(u, R, z) \equiv \int_u^R \frac{\mu(v, z)}{v}dv, \tag{A6}$$

and so, if μ is independent of R,

$$\rho_*\sigma_R^2 = \frac{1}{R^\mu} \int_R^\infty \rho(u, z)\frac{\partial\Phi(u, z)}{\partial u}u^\mu du. \tag{A7}$$

Quite obviously, once the JEs are solved, each adopted ansatz can be expressed in terms of the others. For example, the μ function associated with a b-ansatz is given by

$$\mu = \frac{\Delta_R}{b\sigma_z^2}, \tag{A8}$$

further reducing to $\mu = \Delta/\sigma_z^2$ in the two-integral case, when $b = 1$ and $\Delta_R = \Delta$. Of course, if one adopts the μ-ansatz, the equivalent b is just given by equation (9), where now σ_R^2 is computed as in equation (A5).

An important advantage of using the μ-ansatz should be noticed. From equation (A5), it follows that $\sigma_R^2 \geq 0$ for realistic potentials with $\partial\Phi/\partial R \geq 0$. Therefore, the condition $\mu \geq 1$ in the second of equation (A4) automatically assures the positivity of σ_R^2 and of $\overline{v_\varphi^2}$, without the need for complicated analytical or numerical checks. Therefore, the combination of the μ-ansatz with the generalized Satoh k-decomposition, or better with the most general λ-decomposition, allows for a relatively simple and flexible closure of the JEs.

APPENDIX B: RELATIONS BETWEEN THE REGIONS $\mathscr{B}^\pm$, $\mathscr{C}^\pm$, $\mathscr{D}^\pm$, AND BETWEEN THE LIMITING VALUES FOR b

Some general results about the $\mathscr{B}$, $\mathscr{C}$, and $\mathscr{D}$ regions of axisymmetric systems described by the JEs in Section 3, with $\partial\Phi/\partial R \geq 0$ everywhere, and restricting to $b = b(z)$, are proved.

B1 The ansatz-independent sets

The following ansatz-independent sets, based on the sign of the commutator, are important for the following discussion:

$$\Omega^\pm = \{(R, z) : [\rho_*, \Phi] \gtrless 0\},$$
$$\Omega^0 = \{(R, z) : [\rho_*, \Phi] = 0\}; \tag{B1}$$

we also define $\Omega^{\pm 0} = \Omega^\pm \cup \Omega^0$.

THEOREM B.1. *For all systems, $\mathscr{B}^- \subseteq \mathscr{D}^-$ and $\Omega^- \subseteq \mathscr{D}^-$.*

Proof. Let $P = (R, z) \in \mathscr{B}^-$. From the first of equation (12) and given $\sigma_z^2 \geq 0$, then $P \in \mathscr{D}^-$, and the first inclusion is proved. Let $P = (R, z) \in \Omega^-$. From equation (4) and given $\partial\Phi/\partial R \geq 0$, then $P \in \mathscr{D}^-$, and the second inclusion is proved. From the proved results, it immediately follows that $\mathscr{D}^{+0} \subseteq \mathscr{B}^{+0}$ and $\mathscr{D}^{+0} \subseteq \Omega^{+0}$. $\square$

THEOREM B.2. *If $\mathscr{B}^- \subseteq \Omega^{+0}$, then $\mathscr{B}^- \subseteq \mathscr{C}^+$. If $\mathscr{C}^- \subseteq \Omega^{+0}$, then $\mathscr{C}^- \subseteq \mathscr{B}^+$.*

Proof. Let $P = (R, z) \in \mathscr{B}^-$, and $[\rho_*, \Phi] \geq 0$ there. From the second of equation (13), with $B < 0$ and $[\rho_*, \Phi] \geq 0$, then $P \in \mathscr{C}^+$, and the first part the theorem follows immediately if $[\rho_*, \Phi] \geq 0$ for all points in $\mathscr{B}^-$. The second part is proved similarly by considering $C < 0$ in equation (13). $\square$

THEOREM B.3. *If $\mathscr{B}^{+0} \subseteq \Omega^-$, then $\mathscr{B}^{+0} \subset \mathscr{C}^-$. If $\mathscr{C}^{+0} \subseteq \Omega^-$, then $\mathscr{C}^{+0} \subset \mathscr{B}^-$.*

Proof. Let $P = (R, z) \in \mathscr{B}^+$, and $[\rho_*, \Phi] < 0$ there. From the second of equation (13), with $B \geq 0$ and $[\rho_*, \Phi] < 0$, then $P \in \mathscr{C}^-$, and the first part the theorem follows immediately if $[\rho_*, \Phi] < 0$ for all points in $\mathscr{B}^{+0}$. The second part is proved similarly by considering $C \geq 0$ in equation (13). $\square$

B2 Relations between the limits for b

THEOREM B.4. *For all systems, $b_0(z) \leq b_M(z)$ over the rectangular strip $R \geq 0$ and $z \in \text{Pr}(\mathscr{B}^-)$.*

Proof. From equation (19), $b_M(z)$ is defined over the strip in the (R, z)-plane with $z \in \text{Pr}(\mathscr{B}^-)$, and from equation (21), $b_0(z)$ is defined over the strip with $z \in \text{Pr}(\mathscr{D}^-)$. From Theorem B.1, $\mathscr{B}^- \subseteq \mathscr{D}^-$, so that $b_0(z)$ is certainly defined for $z \in \text{Pr}(\mathscr{B}^-)$. Over $\mathscr{B}^-$, both B and D are negative, so that from the first of equation (12), $|B| = R|D|/\rho_* - \sigma_z^2 \leq R|D|/\rho_*$. It follows that the minimum in the first of equation (19) over $\mathscr{B}_z^-$ is larger than the minimum obtained when $|B|$ is replaced by $R|D|/\rho_*$, and in turn this minimum is larger than that evaluated over the wider set $\mathscr{D}_z^- \supseteq \mathscr{B}_z^-$: from the first of equation (21), this last minimum is the value of $b_0(z)$ for points with $z \in \text{Pr}(\mathscr{B}^-)$, concluding the proof. $\square$

THEOREM B.5. *Let $\mathscr{C}^- \subseteq \Omega^{+0}$, then $b_1(z) \leq 1$ over the rectangular strip $R \geq 0$ and $z \in \text{Pr}(\mathscr{C}^-)$.*

Proof. For assumption $\mathscr{C}^- \subseteq \Omega^{+0}$, so that from Theorem B.2 $\mathscr{B}^+ \cap \mathscr{C}^- = \mathscr{C}^-$, and from equation (23) with $[\rho_*, \Phi] \geq 0$, $b_1(z) \leq 1$ for $z \in \text{Pr}(\mathscr{C}^-)$. $\square$

THEOREM B.6. *Let $\mathscr{B}^- \subseteq \Omega^{+0}$, then $b_2(z) \geq 1$ and $b_0(z) \leq b_2(z) \leq b_M(z)$ over the rectangular strip $R \geq 0$ and $z \in \text{Pr}(\mathscr{B}^-)$.*

Proof. From equation (24) and Theorem B.2, $b_2(z)$ is defined over $\mathscr{B}^- \cap \mathscr{C}^+ = \mathscr{B}^-$, and from the assumed positivity of $[\rho_*, \Phi]$ over $\mathscr{B}^-$, it follows that $b_2(z) \geq 1$, for $z \in \text{Pr}(\mathscr{B}^-)$. Moreover, from Theorem B.4, the functions $b_2(z)$, $b_0(z)$, and $b_M(z)$ are all defined for points with $z \in \text{Pr}(\mathscr{B}^-)$. Again from equation (24), using the inequality $|B| \leq R|D|/\rho_*$ (see the proof of Theorem B.4), and finally from the positivity of the commutator over $\mathscr{B}^-$, it follows that $b_2(z)$ is larger than the minimum of the function appearing in the second of equation (21), now computed over $\mathscr{B}^-$. As $\mathscr{B}^- \subseteq \mathscr{D}^-$ from Theorem B.1, extending this minimum over $\mathscr{D}^-$ further decreases its value, proving that $b_2(z) \geq b_0(z)$. $b_M(z) \geq b_2(z)$ follows by comparison between equations (19) and (24), where $\mathscr{B}^- \cap \mathscr{C}^+ = \mathscr{B}^-$ and $\sigma_z^2 \geq 0$. Notice that $b_0(z)$ can be larger or lower than 1 depending on the sign of $[\rho_*, \Phi]$ over the region $\mathscr{D}^- \cap \mathscr{B}^+$, for $z \in \text{Pr}(\mathscr{B}^-)$. $\square$

THEOREM B.7. *Let $\mathscr{D}^- \subseteq \Omega^{+0}$, then $b_0(z) \geq 1$ over the rectangular strip $R \geq 0$ and $z \in \text{Pr}(\mathscr{D}^-)$, and $1 \leq b_0(z) \leq b_2(z) \leq b_M(z)$ over the strip $z \in \text{Pr}(\mathscr{B}^-) \subseteq \text{Pr}(\mathscr{D}^-)$.*

Proof. By assumption $\mathscr{D}^- \subseteq \Omega^{+0}$, so that from equation (21) $b_0(z) \geq 1$ for $z \in \text{Pr}(\mathscr{D}^-)$. The second part of the theorem descends immediately from the inequality just proved and Theorem B.6, because from Theorem B.1, $\mathscr{B}^- \subseteq \mathscr{D}^-$ ($\subseteq \Omega^{+0}$ by assumption). Notice how strengthening the hypothesis of Theorem B.6 (i.e. $\mathscr{B}^- \subseteq \Omega^{+0}$) to that of the present case ($\mathscr{D}^- \subseteq \Omega^{+0}$) allows to establish whether $b_0(z)$ is larger or smaller than unity, then resolving the indeterminacy mentioned at the end of the proof of Theorem B.6. $\square$

This paper has been typeset from a TEX/LATEX file prepared by the author.